FORMULAS BASICAS
DINAMICA DE ESTRUCTURAS
R. BOROSCHEK

Coordenadas Generalizadas:

$$m^* = \int_0^L m(x)[\phi(x)]^2\,dx + \sum m_i\phi_i^2 + \sum I_{oi}(\phi_i')^2$$

$$k^* = \int_0^L k(x)[\phi]^2\,dx + \sum k_i\phi_i^2 + \int_0^L EI(x)[\phi''(x)]^2\,dx$$

$$c^* = \int_0^L c(x)[\phi(x)]^2\,dx + \sum c_i\phi_i^2$$

$$p^*(t) = \int_0^L p(x,t)\phi(x)\,dx + \sum p_i(t)\phi_i$$

Ecuación de movimiento:

$$m\ddot{v}(t) + c\dot{v}(t) + kv(t) = p(t)$$

Amortiguamiento crítico : $c_c = 2mw$
Razón de amortiguamiento: $\xi = \frac{c}{c_c} = \frac{c}{2mw}$
Frecuencia amortiguada: $w_d = w\sqrt{1-\xi^2}$
Respuesta a condiciones iniciales:

$$v(t) = e^{-\xi wt} \times \left[\frac{\dot{v}(0)+v(0)\xi w}{w_d}\text{sen}(w_d t) + v(0)\cos(w_d t)\right]$$

Respuesta para $p(t) = p_o sen(\bar{w}t)$

$$v(t) = \frac{p_o}{k}D\text{sen}(\bar{w}t - \theta)$$

$$D = \left[(1-\gamma^2)^2 + (2\xi\gamma)^2\right]^{-1/2} \qquad \gamma = \frac{\bar{w}}{w}$$

$$\theta = \tan^{-1}\frac{2\xi\gamma}{1-\gamma^2}$$

Integral de Duhamel:

$$v(t) = \frac{1}{mw_d}\int_0^t p(\tau)e^{-\xi w(t-\tau)}\text{sen}(w_d(t-\tau))d\tau$$

Rayleigh:

$$w^2 = \frac{k^*}{m^*}$$

Sistemas discretos de varios grados de libertad:

Ecuación de movimiento:

$$[\text{M}]\ddot{v}(t) + [\text{C}]\dot{v}(t) + [\text{K}]v(t) = [\text{P}(t)]$$

Coordenadas modales: $v(t) = \sum_{i=1}^{N}[\phi_i]Y_i(t)$

Masa modal: $M_n = [\phi_n^T][\text{M}][\phi_n]$

Rigidez modal: $K_n = [\phi_n^T][\text{K}][\phi_n]$

Fuerza modal: $P_n = [\phi_n^T][\text{P}]$

Condición inicial:

$$Y_n(0) = \frac{[\phi_n^T][\text{M}][v(0)]}{[\phi_n^T][\text{M}][\phi_n]}$$

$\underline{C} = a_o\underline{M} + a_1\underline{K}$ Rayleigh

Análisis espectral:

Factor de participación:

$$L_n = [\phi_n^T][\text{M}][r]$$

Desplazamiento modal:

$$Y_{n\,max} = \frac{L_n}{M_n w_n}PS_v(T_n,\xi_n)$$

Fuerza modal:

$$F_{n\,max} = [\text{M}][\phi_n]\frac{L_n}{M_n}w_n PS_v(T_n,\xi_n)$$

Corte basal modal, edificio de corte:

$$Q_{n\,max} = \frac{L_n^2}{M_n}w_n PS_v(T_n,\xi_n)$$

Sistemas con parámetros distribuidos:
Ecuación de movimiento viga flexión:

$$\frac{\partial^2}{\partial x^2}\left(EI(x)\frac{\partial^2 v(x,t)}{\partial x^2}\right) + m(x)\frac{\partial^2 v(x,t)}{\partial t^2} = p(x,t)$$

Solución:

$$v(x,t) = \sum_{i=1}^{\infty}\phi_i(x)Y_i(t)$$

Ortogonalidad:

$$\int_0^L \phi_m(x)\phi_n(x)m(x)dx = 0$$

$$\int_0^L \phi_m(x)\frac{d^2}{dx^2}\left[EI(x)\frac{d^2\phi_n(x)}{dx^2}\right]dx = 0$$

$$\phi_m(x)V_n(x)\Big|_0^L - \phi_m' M_n(x)\Big|_0^L +$$
$$+ \int_0^L \phi_m''(x)\phi_n''(x)EI(x)dx = 0$$

REPASO NUMEROS COMPLEJOS

REPRESENTACION

$$a + bi$$

donde:
$i^2 = -1$
a, b números reales

Suma y resta:

$$(a + bi) \pm (c + di) = (a \pm c) + (b \pm d)i$$

Multiplicación:

$$(a + bi)(c + di) = (ac - bd) + (ad + bc)i$$

División:

$$\frac{a + bi}{c + di} = \frac{ac + bd}{c^2 + d^2} + \frac{bc - ad}{c^2 + d^2}i$$

REPRESENTACION POLAR

$$x + iy = r(\cos(\theta) + i\text{sen}(\theta))$$

donde:
$r = \sqrt{x^2 + y^2}$
$\theta = \arctan(y/x)$

Multiplicación:

$$[r_1(\cos(\theta_1) + i\text{sen}(\theta_1))][r_2(\cos(\theta_2) + i\text{sen}(\theta_2))] = r_1 r_2[\cos(\theta_1 + \theta_2) + i\text{sen}(\theta_1 + \theta_2)]$$

División:

$$\frac{r_1(\cos\theta_1 + i\text{sen}\theta_1)}{r_2(\cos\theta_2 + i\text{sen}\theta_2)} = \frac{r_1}{r_2}[\cos(\theta_1 - \theta_2) + i\text{sen}(\theta_1 - \theta_2)]$$

Potencia: Teorema de De Moivre

$$[r(\cos(\theta) + i\text{sen}(\theta))]^p = r^p(\cos(p\theta) + i\text{sen}(p\theta))$$

donde:
p es un número real.

Raíz:

$$[r(\cos(\theta) + i\text{sen}(\theta))]^{1/n} = r^{1/n}\left(\cos\left(\frac{\theta + 2k\pi}{n}\right) + i\text{sen}\left(\frac{\theta + 2k\pi}{n}\right)\right)$$

donde:
n es entero positivo.
k es entero positivo y $k = 0, 1, 2, ..., n-1$

REPRESENTACION EXPONENCIAL

$$x + iy = r(\cos(\theta) + i\text{sen}(\theta)) = re^{i\theta}$$

Multiplicación:

$$(r_1 e^{i\theta_1})(r_2 e^{i\theta_2}) = r_1 r_2 e^{i(\theta_1 + \theta_2)}$$

División:

$$\frac{r_1 e^{i\theta_1}}{r_2 e^{i\theta_2}} = \frac{r_1}{r_2} e^{i(\theta_1 - \theta_2)}$$

Potencia (teorema De Moivre) :

$$(re^{i\theta})^p = r^p e^{ip\theta}$$

Raíz:

$$(re^{i\theta})^{1/n} = r^{1/n} e^{i\left(\frac{\theta + 2k\pi}{n}\right)} \quad k = 1, 2, ...n-1$$

Logaritmo:

$$\ln(re^{i\theta}) = \ln r + i\theta + 2k\pi i \quad k = \text{entero}$$

Relación entre exponencial compleja y función trigonométrica

Identidades de Euler:

$$e^{\pm i\theta} = \cos\theta \pm i\text{sen}\theta$$

$$\text{sen}\theta = \frac{e^{i\theta} - e^{-i\theta}}{2i}$$

$$\cos\theta = \frac{e^{i\theta} + e^{-i\theta}}{2}$$

$$\tan\theta = -i\frac{e^{i\theta} - e^{-i\theta}}{e^{i\theta} + e^{-i\theta}}$$

$$\cot\theta = i\frac{e^{i\theta} + e^{-i\theta}}{e^{i\theta} - e^{-i\theta}}$$

$$\sec\theta = \frac{2}{e^{i\theta} + e^{-i\theta}}$$

$$\csc\theta = \frac{2i}{e^{i\theta} - e^{-i\theta}}$$

Otras relaciones:

$$\operatorname{sen}(ix) = i\operatorname{senh}(x)$$

$$\csc(ix) = -i\operatorname{csch}(x)$$

$$\cos(ix) = \cosh(x)$$

$$\sec(ix) = \operatorname{sech}(x)$$

Uniform rod

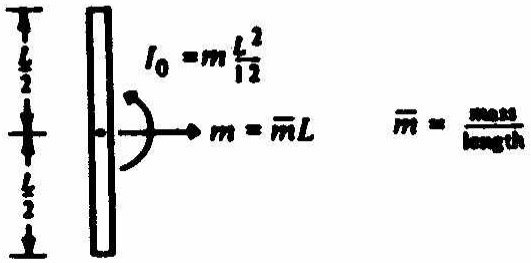

Uniform plates

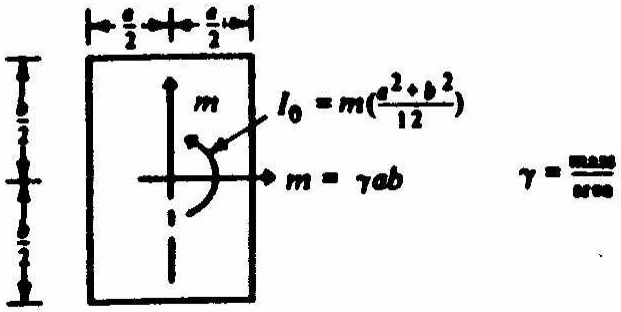

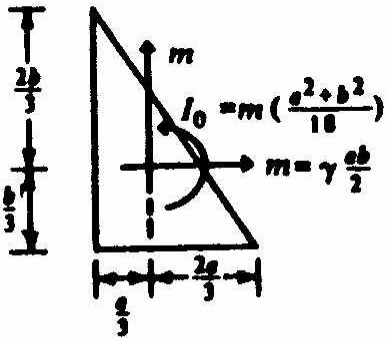

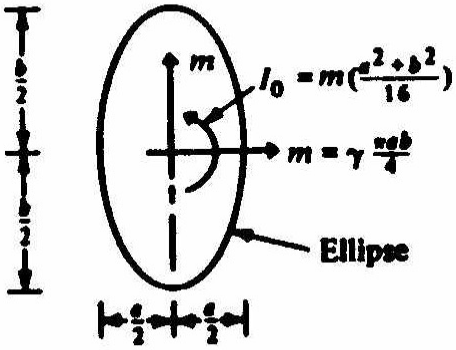

FIGURE 2-4
Rigid-body mass and mass moment of inertia.

$$f = \frac{\omega}{2\pi}$$

$$\frac{1}{f} = \frac{2\pi}{\omega} = T$$

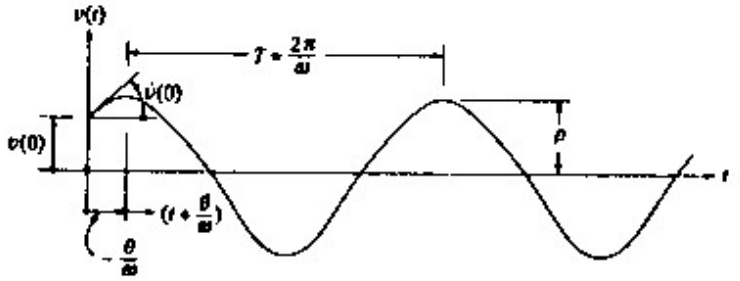

$$v(t) = v(0)\cos\omega t + \frac{\dot{v}(0)}{\omega}\sin\omega t$$

FIGURE 1-7
Undamped free-vibration response.

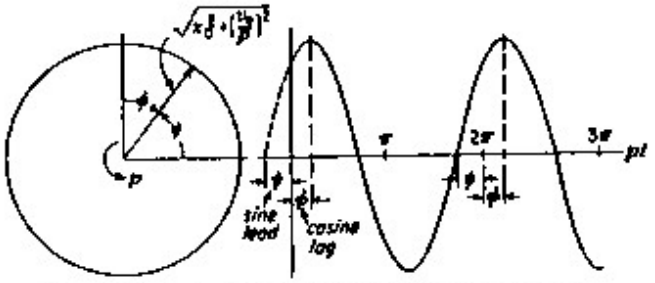

FIG. 1-17. Angle or time projection of resultant vector.

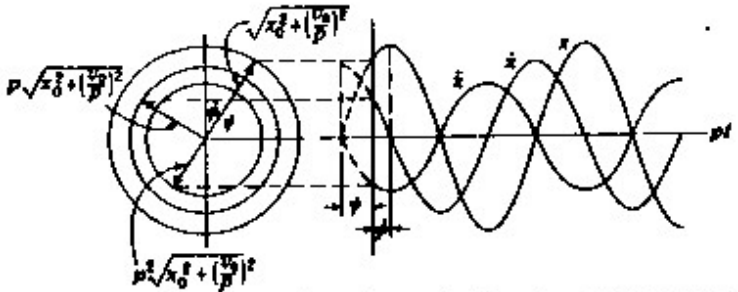

FIG. 1-18. Relations as well as angle or time projection of vectors of displacement, velocity, and acceleration.

$$\left.\begin{matrix}\dot{z}\\ z\end{matrix}\right\} = \sqrt{x_0^2 + \frac{v_0^2}{p^2}} \left\{\begin{matrix}-p\sin(pt-\phi)\\ -p^2\cos(pt-\phi)\end{matrix}\right. \qquad (1\text{-}4a)$$

$$\left.\begin{matrix}\dot{z}\\ z\end{matrix}\right\} = \sqrt{x_0^2 + \frac{v_0^2}{p^2}} \left\{\begin{matrix}p\cos(pt+\psi)\\ -p^2\sin(pt+\psi)\end{matrix}\right. \qquad (1\text{-}4b)$$

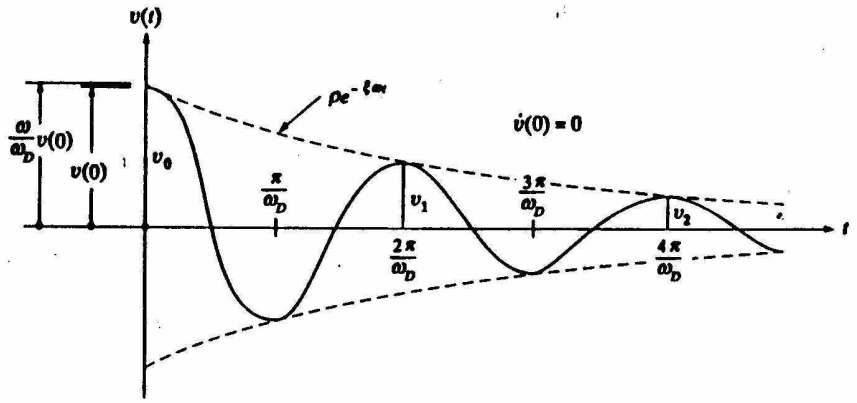

$$v(t) = \rho \cos(\omega_D t + \theta) \exp(-\xi\omega t)$$

$$\rho = \left\{ v(0)^2 + \left(\frac{\dot{v}(0) + v(0)\xi\omega}{\omega_D} \right)^2 \right\}^{1/2}$$

$$\theta = -\tan^{-1}\left(\frac{\dot{v}(0) + v(0)\xi\omega}{\omega_D\, v(0)} \right)$$

FIGURE 2-11
Free-vibration response of undercritically-damped system.

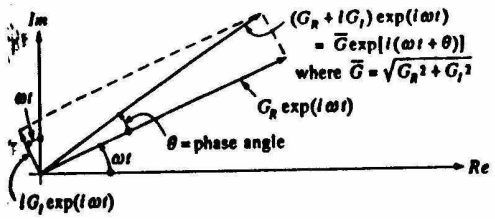

FIGURE 2-5
Portrayal of first term of Eq. (2-29).

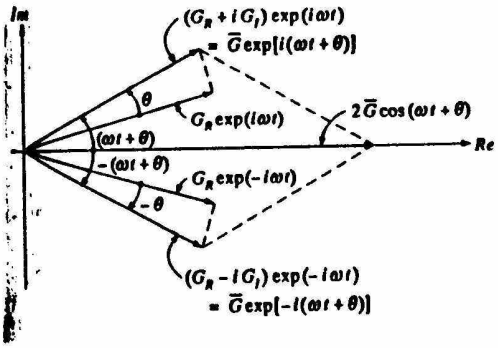

FIGURE 2-6
Total free-vibration response.

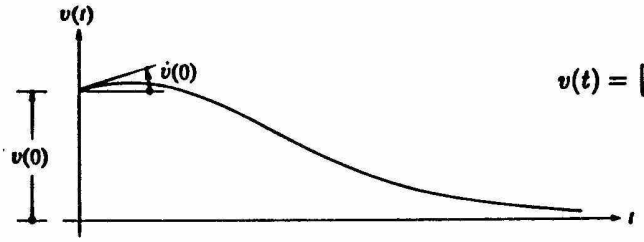

$$v(t) = \left[v(0)\,(1 - \omega t) + \dot{v}(0)\, t \right] \exp(-\omega t)$$

FIGURE 2-9
Free-vibration response with critical damping.

Summary of Gain Factors for Simple Mechanical System

Values for the Gain Factor $\lvert H(f)\rvert$ of a Simple Mechanical System as a Function of the Input and Output Parameters		Foundation Motion Input (see Fig. 2.4 for model)			Force Input (see Fig. 2.2 for model)
		Displacement $x(t)$ in.	Velocity $\dot{x}(t)$ in./sec	Acceleration $\ddot{x}(t)$ in./sec^2	Force (in displacement units) $x(t) = F(t)/k$ in.
In terms of displacement output, in.	Absolute displacement $y(t)$	$\frac{D_1}{D_2}$	$\frac{D_1}{2\pi f D_2}$	$\frac{D_1}{4\pi^2 f^2 D_2}$	$\frac{1}{D_2}$
	Relative displacement $z(t) = y(t) - x(t)$	$\frac{f^2}{f_n^2 D_2}$	$\frac{f}{2\pi f_n^2 D_2}$	$\frac{1}{4\pi^2 f_n^2 D_2}$	
In terms of velocity output, in./sec.	Absolute velocity $\dot{y}(t)$	$\frac{2\pi f D_1}{D^2}$	$\frac{D_1}{D_2}$	$\frac{D_1}{2\pi f D_2}$	$\frac{2\pi f}{D_2}$
	Relative velocity $\dot{z}(t) = \dot{y}(t) - \dot{x}(t)$	$\frac{2\pi f^3}{f_n^2 D_2}$	$\frac{f^2}{f_n^2 D_2}$	$\frac{f}{2\pi f_n^2 D_2}$	
In terms of acceleration output, in./sec^2.	Absolute acceleration $\ddot{y}(t)$	$\frac{4\pi^2 f^2 D_1}{D^2}$	$\frac{2\pi f D_1}{D^2}$	$\frac{D_1}{D_2}$	$\frac{4\pi^2 f^2}{D_2}$
	Relative acceleration $\ddot{z}(t) = \ddot{y}(t) - \ddot{x}(t)$	$\frac{4\pi^2 f^4}{f_n^2 D_2}$	$\frac{2\pi f^3}{f_n^2 D_2}$	$\frac{f^2}{f_n^2 D_2}$	

$D_1 = \sqrt{1 + [2\zeta(f/f_n)]^2}$ $\quad D_2 = \sqrt{[1 - (f/f_n)^2]^2 + [2\zeta(f/f_n)]^2}$

$f_n = \frac{1}{2\pi}\sqrt{\frac{k}{m}}$ $\quad \zeta = \frac{c}{2\sqrt{km}}$

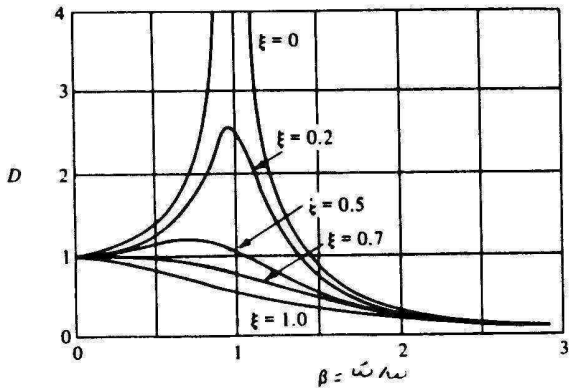

FIGURE 4-4
Variation of dynamic magnification factor with damping and frequency.

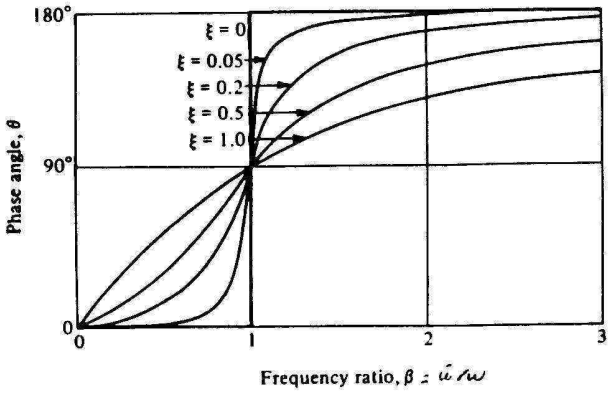

FIGURE 4-5
Variation of phase angle with damping and frequency.

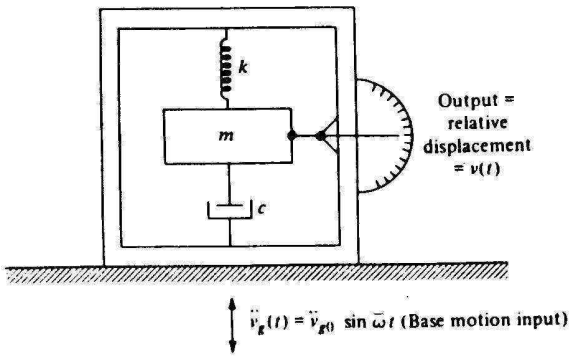

FIGURE 4-8
Schematic diagram of a typical seismometer.

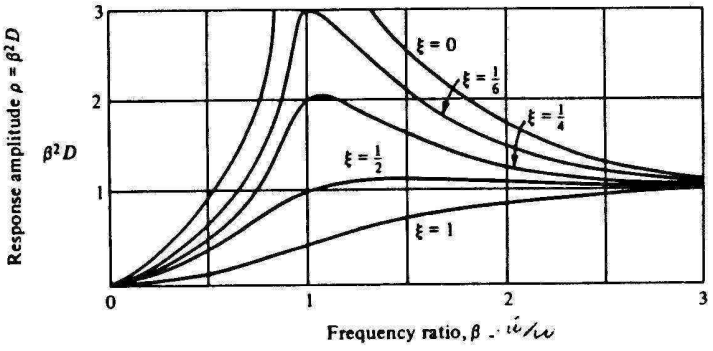

FIGURE 4-9
Response of seismometer to harmonic base displacement

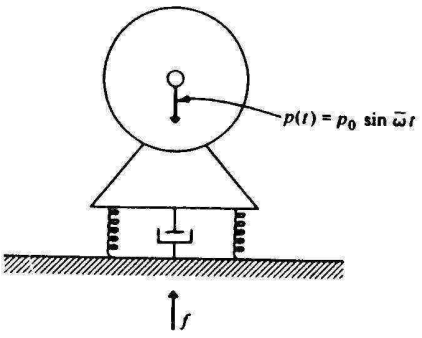

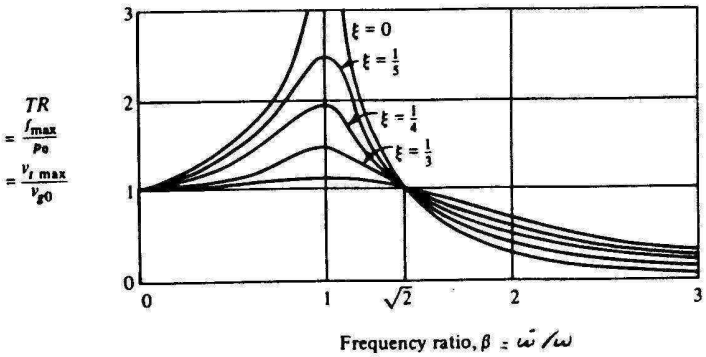

FIGURE 4-11
Vibration-transmissibility ratio (applied load or displacement).

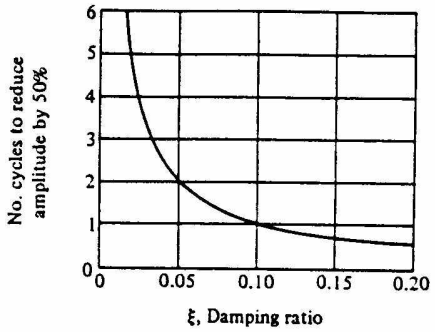

FIGURE 3-8
Damping ratio vs. number of cycles required to reduce amplitude by 50 percent.

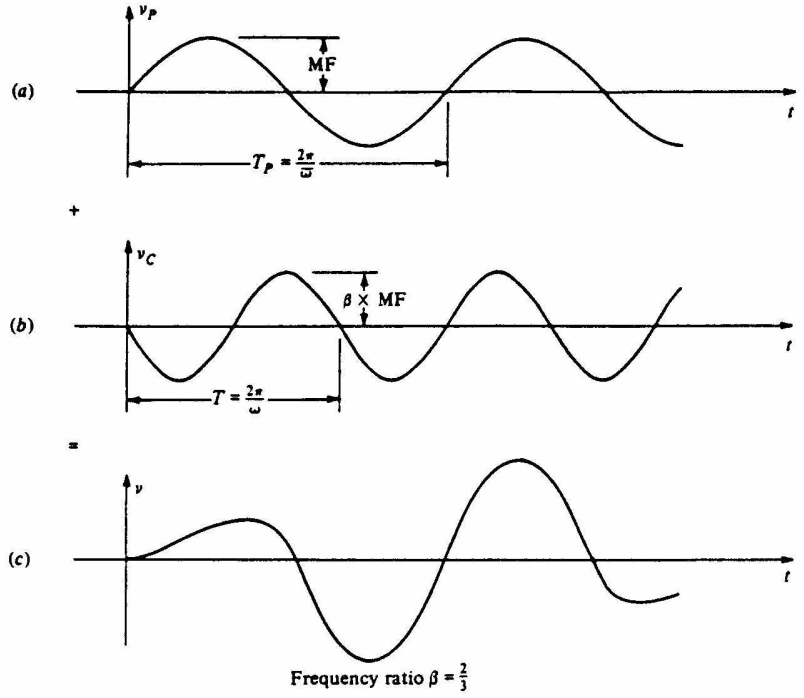

FIGURE 4-1
Response to harmonic load from at-rest initial conditions: (*a*) steady state; (*b*) transient; (*c*) total $R(t)$.

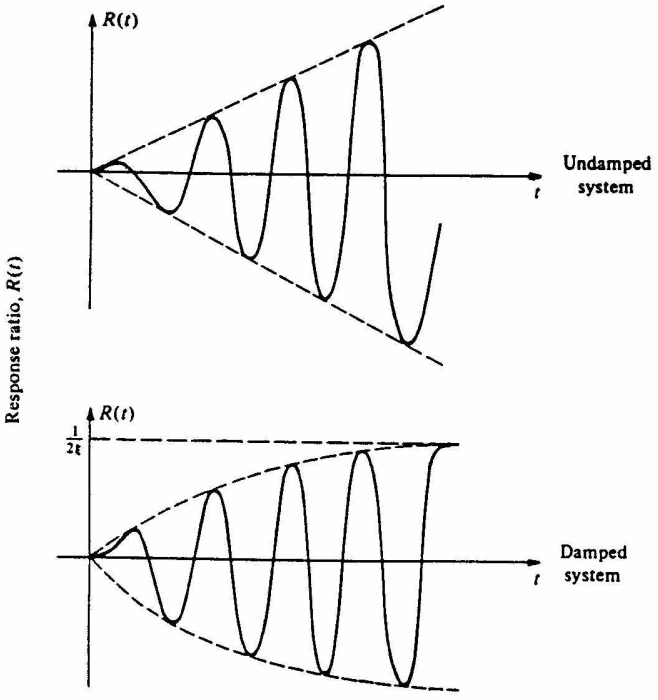

FIGURE 4-6
Response to resonant loading $\beta = 1$ for at-rest initial conditions.

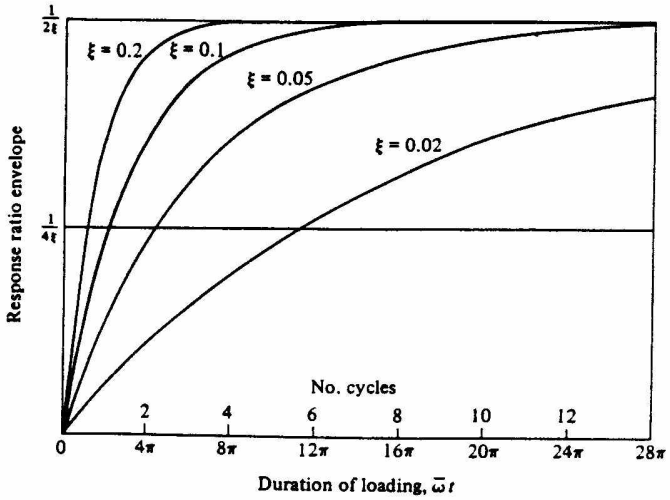

FIGURE 4-7
Rate of buildup of resonant response from rest.

ESPECTRO FUERZA IMPULSIVA O IMPACTO

(Clough - Penzien, 1975)

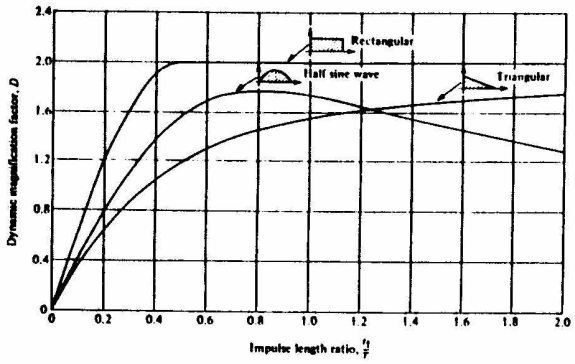

FIGURE 6-6
Displacement-response spectra (shock spectra) for three types of impulse.

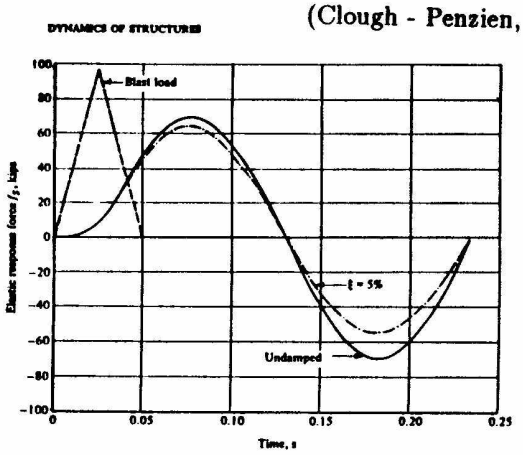

FIGURE E7-2
Response of water tower to blast load.

EJEMPLO GRAFICO DE LA INTEGRAL DE CONVOLUCION

$y(t) = x(t) * h(t)$

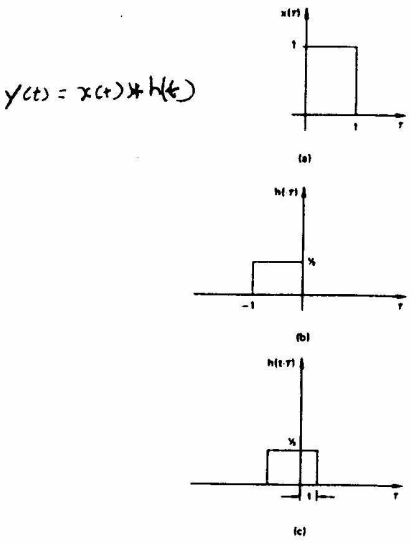

Figure 4-2. Graphical description of folding operation.

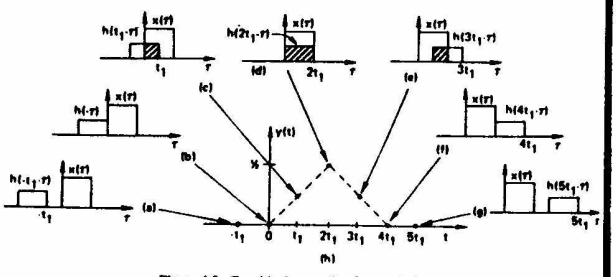

Figure 4-3. Graphical example of convolution.

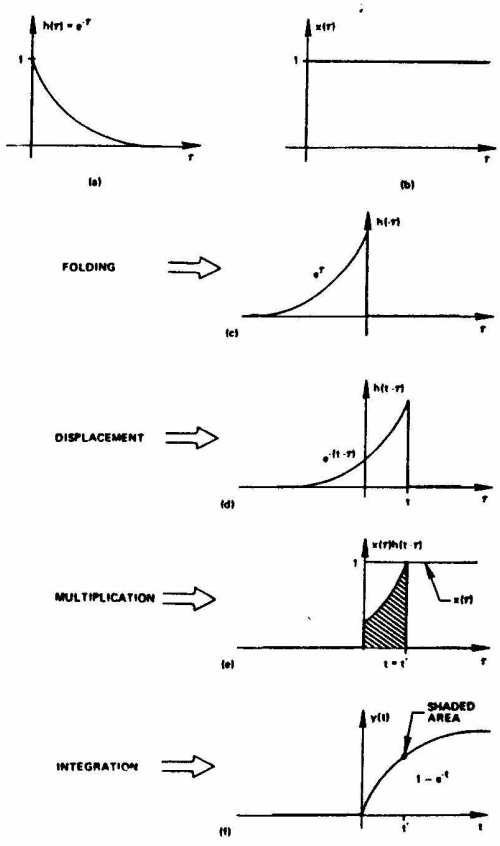

Figure 4-4. Convolution procedure: folding, displacement, multiplication, and integration.

(Brigham, 1974)

INSTRUMENTOS PARA LA MEDICION DE VIBRACIONES SISMICAS

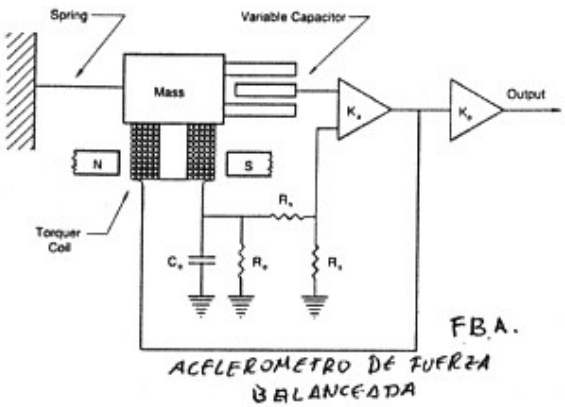

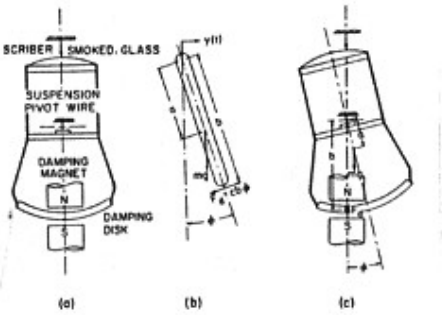

Fig. 6.12. Schematic diagram of USCGS seismoscope. (From Cloud and Hudson, 1961.)

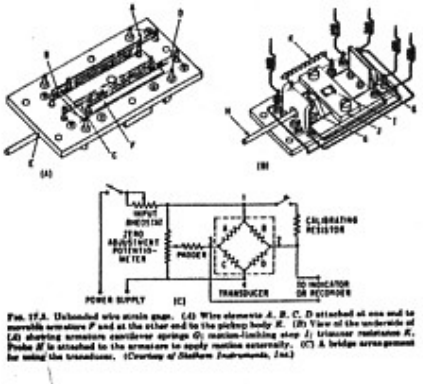

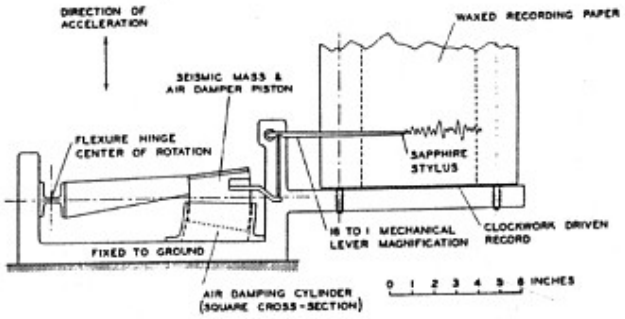

Fig. 6.6. Schematic diagram of SMAC accelerograph. (From Hud-

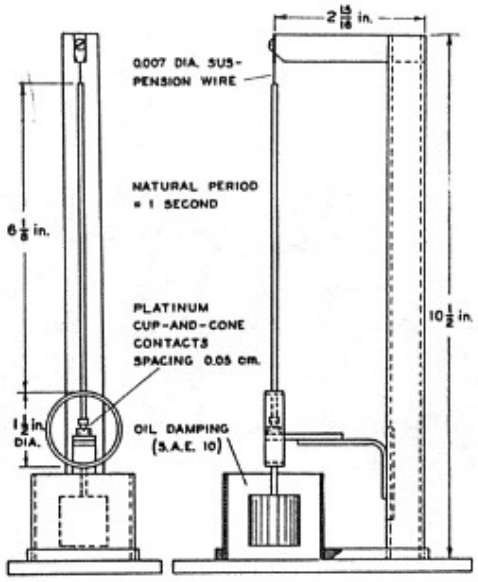

Fig. 6.8. Pendulum starter for the USCGS accelerograph. (From Hudson, 1963.)

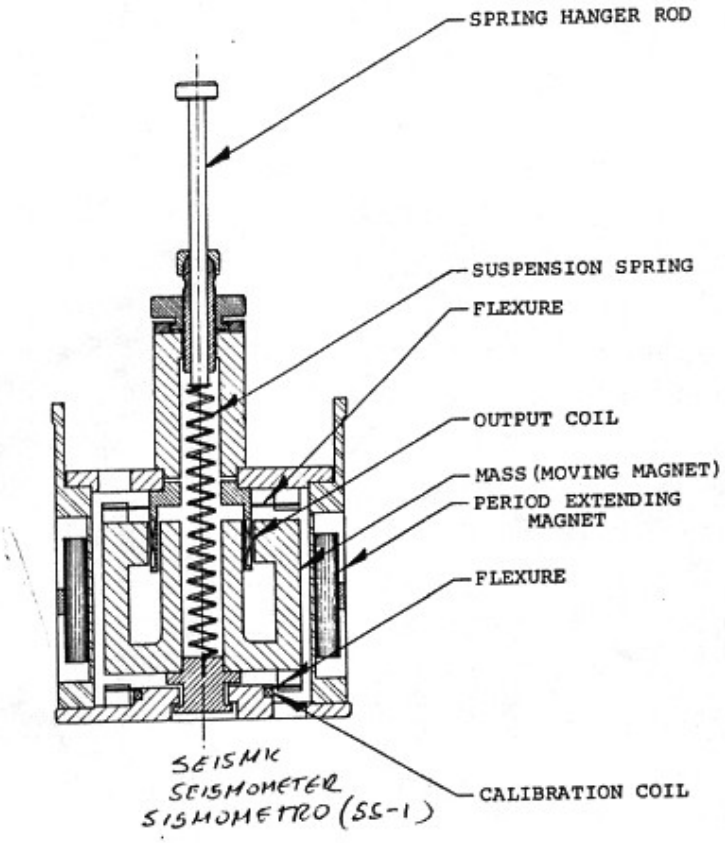

Fig. 7.9. Four synchronized vibration generators exciting an earth-filled dam. (From Keightley, 1966.)

Fig. 7.6. Counterrotating eccentric weight vibration generator. (From Hudson, 1964.)

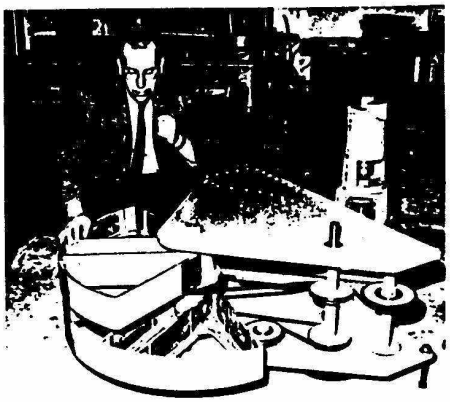

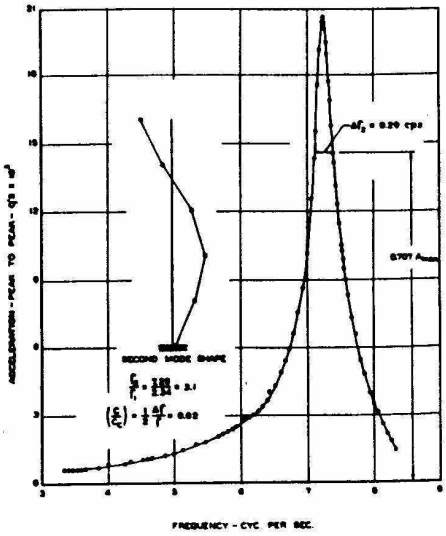

Fig. 7.2. Resonance test of a five-story reinforced concrete building. (From Hudson, 1964.)

Fig. 7.3. Hysteresis-type resonance curves. (From Jennings, 1964.)

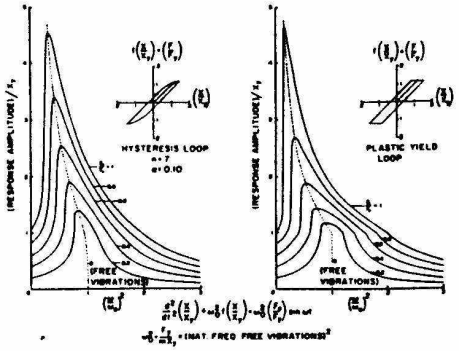

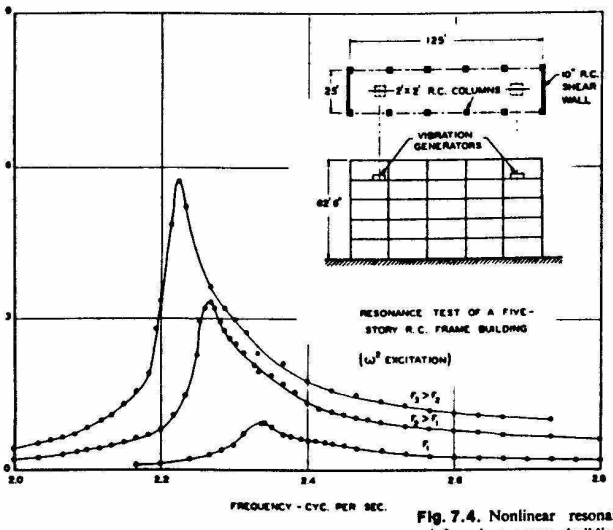

Fig. 7.4. Nonlinear resonance in a reinforced concrete building. (From Hudson, 1964.)

Fig. 7.10. Resonance curves for an earth-filled dam. (From Keightley, 1966.)

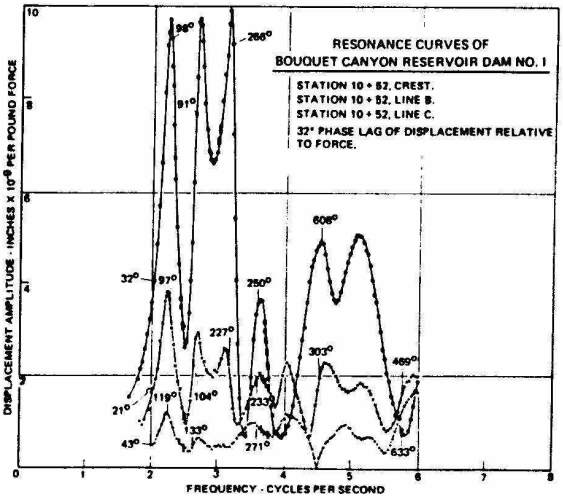

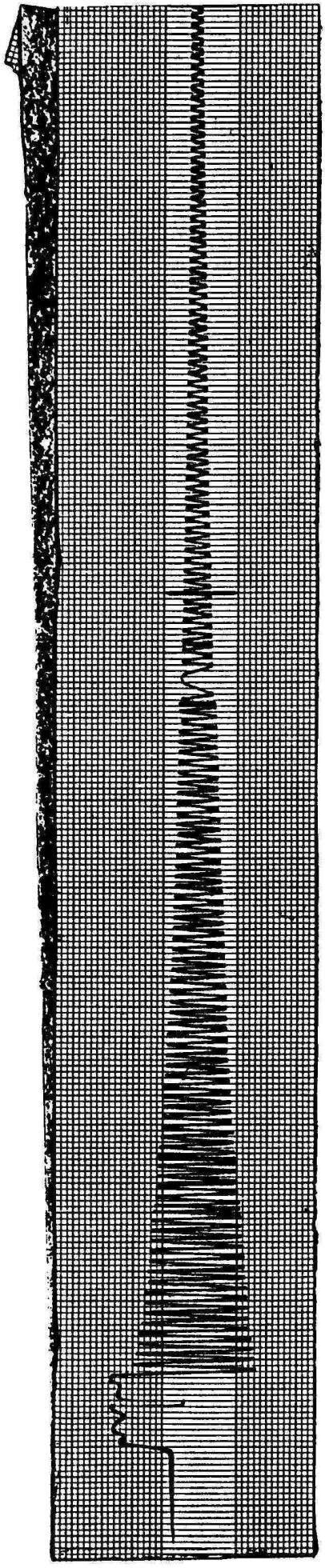

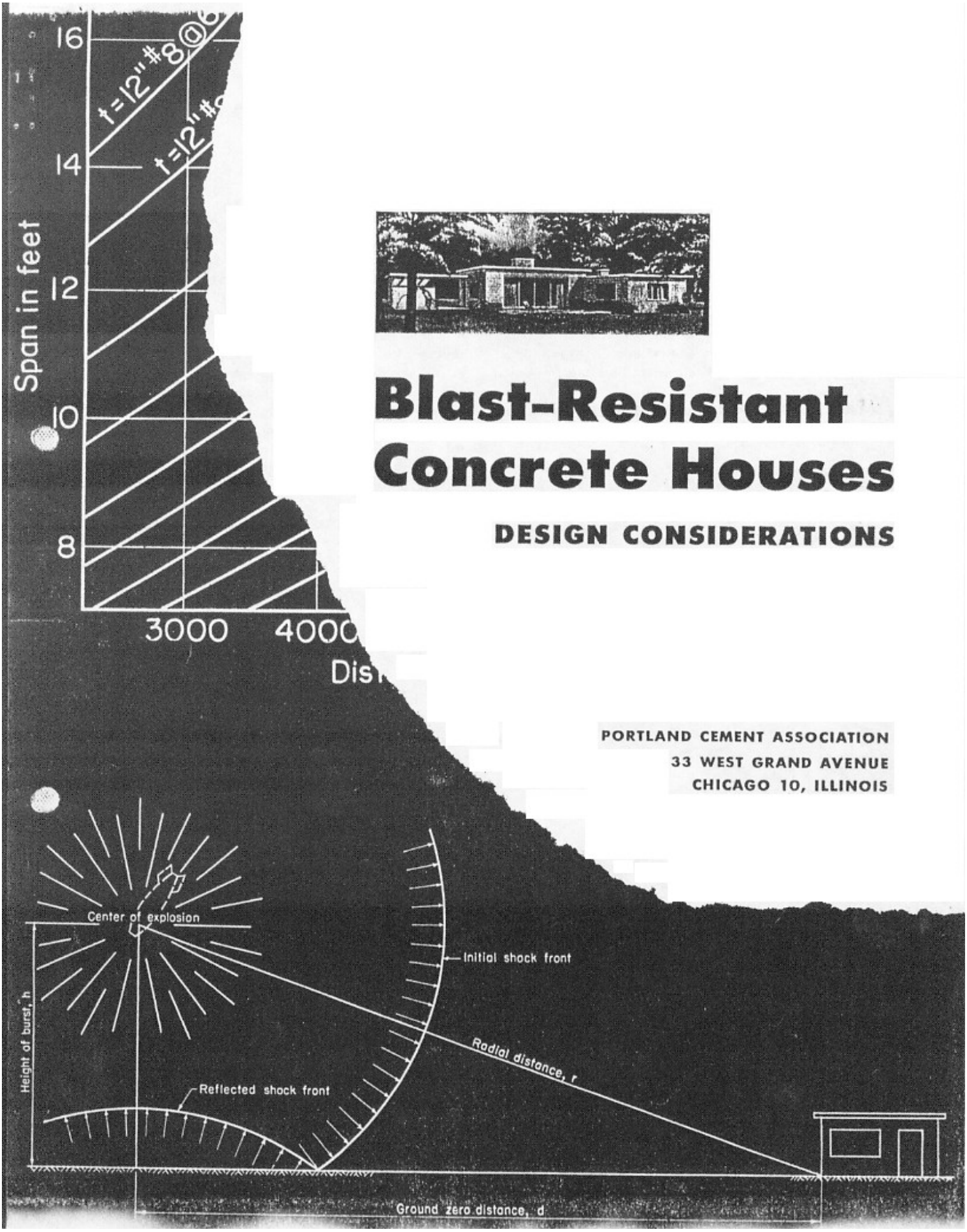

Blast-Resistant Concrete Houses

DESIGN CONSIDERATIONS

PORTLAND CEMENT ASSOCIATION
33 WEST GRAND AVENUE
CHICAGO 10, ILLINOIS

Blast-Resistant Concrete Houses
Design Considerations

Introduction

Extensive investigations and tests show that it is possible to design and build houses to withstand pressures from nuclear blast. Concrete construction will give protection with only little additional cost and without sacrificing the function or appearance of a home.

This publication presents a simplified description of blast loading as it affects one-story houses* in order to provide a clear understanding of the fundamental problems involved.

Shock Wave and Reflected Pressure

When a nuclear bomb explodes above ground, a shock wave of decreasing intensity leaves the center of explosion with an initial speed several times the speed of sound (15,000 ft. per second at "breakaway") and travels outward with a diminishing velocity that approaches the normal speed of sound of 1,100 ft. per second. Fig. 1 shows the location of the shock front after a certain interval of time and its relationship to the structure. The distance between the structure and the center of explosion is determined by the height of burst above ground, *h*, and by the distance, *d*, from ground zero, the point directly below the center of explosion.

The shock front, which presents a rapidly expanding spherical surface, is characterized by an abrupt increase in pressure. The intensity and duration of this pressure can be predicted quite accurately if no interference to the shock front occurs.

Because a bomb is detonated above ground, a reflected shock front develops. The reflected wave, as indicated in Fig. 1, adds to the intensity of the initial shock front. At some distance

*Data in this publication are based on studies made for the Portland Cement Association by Ammann & Whitney, consulting engineers, New York and Milwaukee; and Ellery Husted of Gugler, Kimball and Husted, architects, New York. Both consultants have had extensive experience with various governmental agencies in the field of blast-resistant construction and the effects of nuclear weapons.

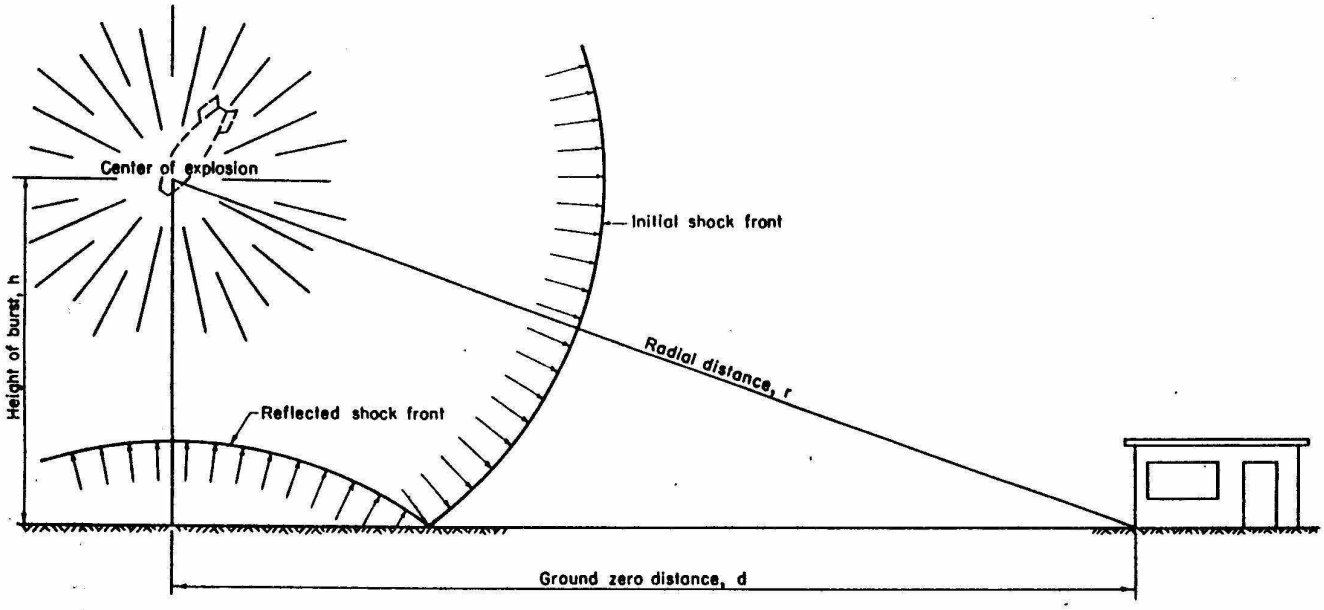

Fig. 1. Geometric relationship between center of explosion, shock front and structure.

the two shock fronts fuse together near the ground, as shown in Fig. 2. The height of this fused shock front increases as it moves outward. The front is approximately vertical and sweeps over the surrounding area with an intensity corresponding to a bomb of twice the yield of the actual one. The pressure in the combined shock wave is generally referred to as the side-on pressure and is denoted as p_s. Its intensity is dependent on distance from ground zero, height of burst and bomb yield.

As the shock front moves forward, the peak side-on pressure, denoted as p_s^p, decreases as indicated by the dash line in Fig. 3. For a 20-KT* bomb, such as that dropped on Hiroshima, the peak side-on pressure at ground zero is about three and one-half times the atmospheric pressure, 14.7 psi; at 2,000 ft. from ground zero it reduces to about 24 psi; and at 9,000 ft. it is, approximately, one-sixth the atmospheric pressure.

For a constant ratio of h to d the distance at which the peak side-on pressure exerted by any other bomb size is approximately equal to the pressure exerted by a 20-KT bomb at a distance d_n is given by the hydrodynamical equation

$$d = d_n \sqrt[3]{\frac{W}{20}}$$

in which

d = the horizontal distance from ground zero for a bomb W;
d_n = the horizontal distance from ground zero for a nominal bomb;
W = yield of the bomb in KT.

For example, the pressure exerted by a 160-KT bomb at a distance of $d = d_n \sqrt[3]{\frac{160}{20}} = 2d_n$ is the same as the pressure exerted by a 20-KT bomb at the distance d_n.

The distribution of pressure behind the fused shock front at two different distances is plotted in Fig. 3 as solid lines under the dash line. In these cases the pressure decreases from the peak side-on value at the designated point to a total less than atmospheric pressure at some distance behind. As the shock wave travels outward, the distance, d_o, subjected to positive pressures increases and the peak intensity decreases.

The pressure conditions that exist when a blast hits a building are indicated in Figs. 4 and 5. The pressure on the front wall facing the blast builds up because of interference with the forward movement of the shock front. This might be described as a piling up of energy. The intensity of the shock wave reflected from the front wall depends on the initial side-on pressure, the width and height of the wall and the angle of incidence measured as the angle between the direction of the blast wave and the normal to the wall surface. Under very unfavorable conditions the reflected pressure could be as much as four or more times the side-on pressure. This build-up of pressure applies mainly to the lateral forces that act on the wall facing the blast.

Near the top of the wall the reflected shock wave travels upward and causes turbulence over the roof. At the front edge of the roof the vertical pressure is approximately the same as the initial side-on pressure. Beyond the edge, however, the pressure drops to a value far below p_s. At a horizontal distance about three times the height of the wall, the turbulence decreases and the pressure again approaches p_s. A similar but much smaller effect takes place near the rear edge of the roof.

*Kiloton or 1,000 tons. A 20-KT bomb, which has roughly the effective energy release of 20,000 tons of TNT, is considered nominal.

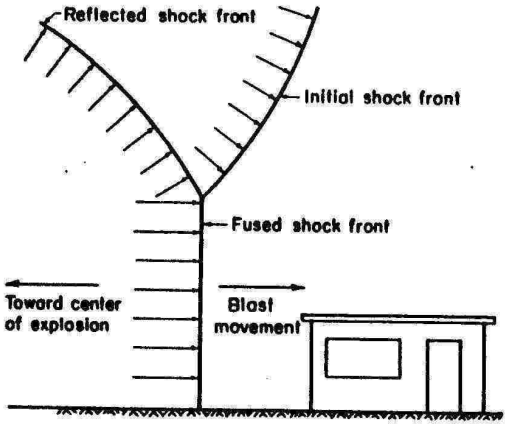

Fig. 2. Formation of a fused shock front.

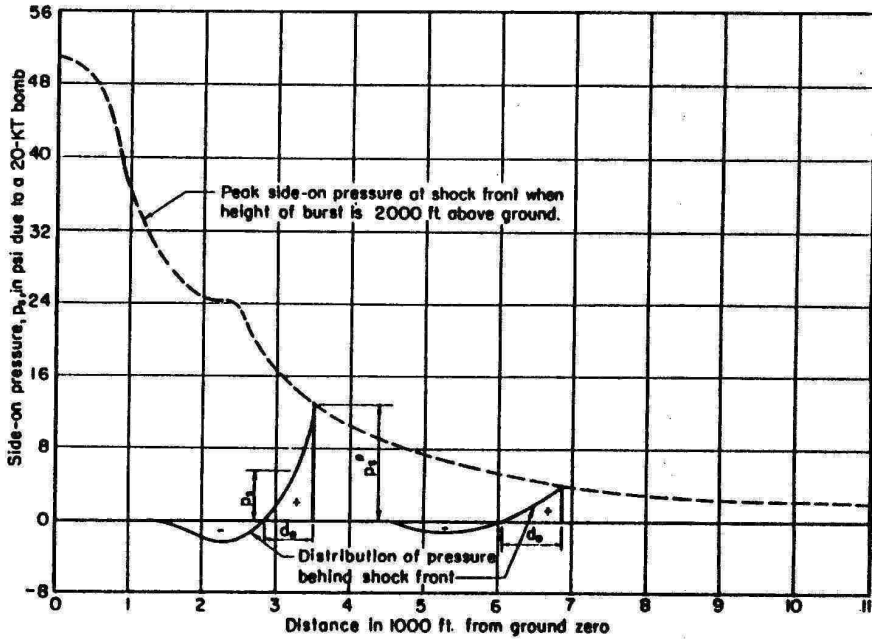

Fig. 3. Peak pressure on the ground as a function of distance from ground zero for a nominal bomb exploded 2,000 ft. above ground.

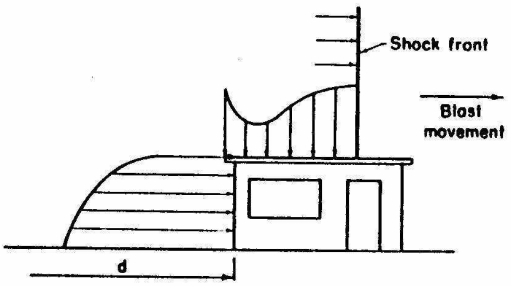

Fig. 4. Blast load on a partially engulfed building.

After the shock front has passed the building, a pressure builds up on the rear wall that, at its maximum, is slightly less than the value of p_s, as indicated in Fig. 5.

The great variety of pressures that may exist around a building, all varying with time, are derived from the initial side-on pressure. They also depend on intensity and duration of blast and on the size, shape and orientation of the structure.

Duration of Peak Pressure

As pointed out in connection with Fig. 3, the side-on pressures immediately behind the shock front decrease. Therefore, in contrast to ordinary static loads, the pressures exerted on a building decrease with time, as shown in Fig. 6. As the blast moves by the building, it goes through a positive phase in which the pressures are greater than atmospheric pressure. After a relatively short time, the blast enters a negative phase of longer duration which, because of its lower intensity, is frequently disregarded in design. The change in pressure during the positive phase may be approximated roughly with a straight line. The time, t_o, is the duration of the positive phase of the blast load, which for a nominal bomb will vary from ½ to 1 second, depending on the distance of the structure from the bomb.

This rather simple pressure-time relationship is complicated by the previously described build-up of shorter-duration reflected pressures on the front face of the front wall and by pressures that exist on the inside face of the wall. Actually, the positive phase of blast pressures cannot be represented by a single straight line. An idealized pressure-time diagram for a front wall located at the distances under consideration is approximated in Fig. 7 by two straight lines. It consists of a

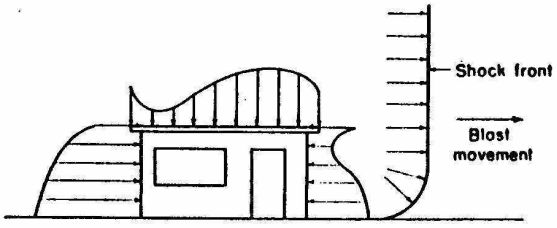

Fig. 5: Blast load on a fully engulfed building.

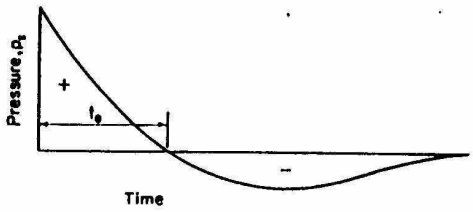

Fig. 6. Pressure-time curve at a given location.

short-duration peak load followed by a smaller drag load of longer duration. Peak load includes reflected side-on pressures. Its duration, t_r, is dependent primarily on the time it takes for a wave to travel three times the height of the wall or one and one-half times its unbroken width, whichever is smaller, at a speed approximately that of normal sound travel. For this reason the duration of peak-load pressures is very sensitive to the geometry of the building. The lower straight line represents the effect of drag on the structure. The total duration of loadings is approximately t_o, but from a strength consideration of the panels, the critical duration is dependent mainly on t_r.

For extremely narrow members such as poles and free-standing columns, the duration of reflected pressures, as shown in Fig. 8, is sharply reduced as compared with the longer duration shown in Fig. 7. The duration, t_r, is so short that the effect of the peak load is negligible and the critical loading is due to drag.

Blast Load on a Structure

Even if all necessary data were available for the calculation of the blast load exerted on a building with openings, such a determination would not be warranted in the case of small buildings because of the number of variables involved. However, a qualitative understanding of the effect of openings can be gathered from test observations.

In the nuclear explosion at the Yucca Flat, Nev., testing ground on May 6, 1955, four houses of reinforced concrete

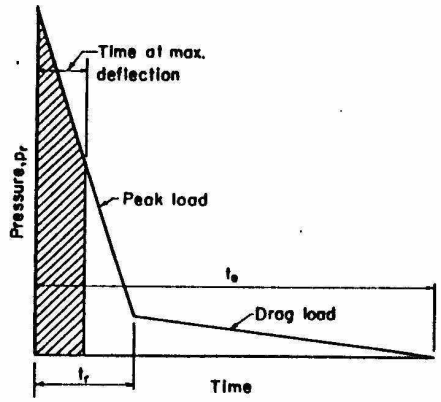

Fig. 7. Simplified pressure-time curve for members of large width and height.

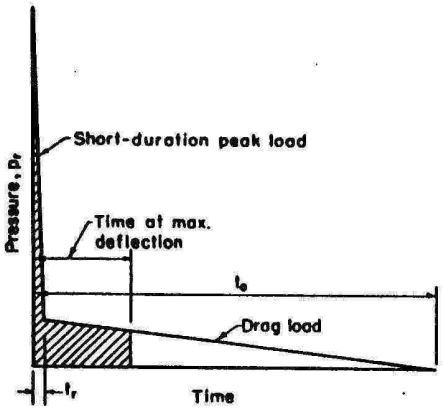

Fig. 8. Simplified pressure-time curve for members of narrow width.

were exposed to blast pressures. The houses were constructed in accordance with ordinary requirements for earthquake resistance.* Two were located 4,700 ft. and two at 10,500 ft. from ground zero. At 4,700 ft. one house of reinforced concrete masonry and another of precast lightweight reinforced concrete withstood the blast of a 35-KT bomb, exploded at a height of 500 ft. The equivalent distance from ground zero in the case of a nominal bomb exploded 2,000 ft. above ground can be shown to be approximately 6,000 ft.** The minimum safe distance for a windowless house can be shown by theoretical investigations to be approximately 11,000 ft. The decrease in safe distance, as proven by the test, can be credited to the relieving effect of wall openings and to the orientation of the structure. These effects are illustrated in Fig. 9.

If a wall is placed parallel to the blast, as shown in Fig. 9(a), it will get very little unbalanced load. The pressure merely engulfs it and is in equilibrium at any time. When a wall is perpendicular to the blast, as in Fig. 9(b), the reflected pressures, p_r, on the front face will build up from two to more than four times† the value of the side-on pressure, p_s. If a wall has windows, the shock front enters and immediately begins to exert pressure on the back of the wall, as shown in Fig. 9(c). The net load on the wall is equal to the difference in load on the two sides.

The duration of the peak pressure on a windowless structure usually will be relatively long since large, unbroken wall areas slow down the escape of reflected pressure. The strength of the front wall of a windowless house must be adequate to resist the peak load, as shown in Fig. 7.

A house with large window areas has a different type of loading curve. After the windows are blown in and only piers and spandrels remain, a quick escape of the reflected pressures is possible. In extreme cases only the drag part of the load diagram shown in Fig. 8 will be effective as load on the structure. The condition encountered in one-story houses is somewhere between the two extremes.

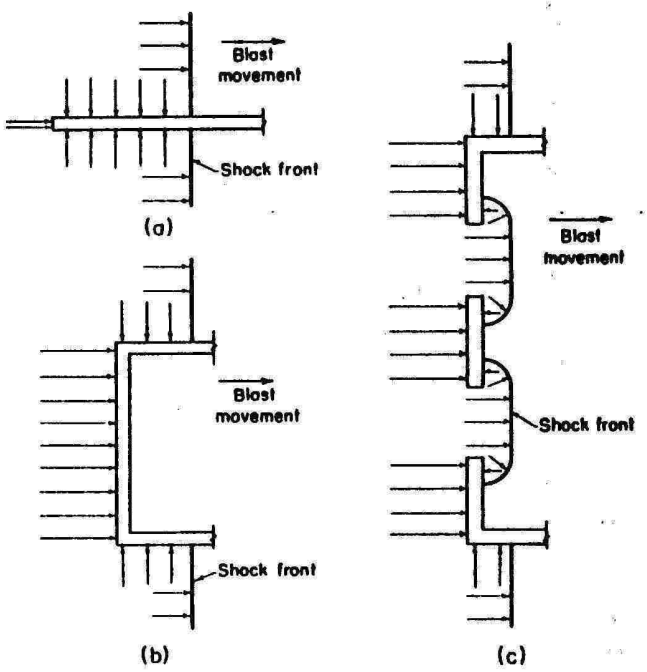

Fig. 9. Pressure on walls of different configurations.

General Layout

Except in those areas in which full protection against blast is required, the house should be laid out in such a way that it will pick up as little of the blast load as possible. Walls without structural function should be made friable, that is, capable of collapsing under the impact of a shock wave without transmitting more than a negligible part of the load to the structural frame. In this category belong light and brittle curtain walls, and ordinary doors and windows.

In many cases the blast direction can be predicted. In a suburb the direction is usually toward an industrial area or the city center. The main structural walls should preferably be made parallel to the blast direction and all other walls should be provided with large windows. The side-on pressures would then tend to equalize each other on the two faces of the structural walls. Openings in these should be kept to a minimum to provide maximum strength.

If the blast direction is not known, a wall may be subject to either full lateral reflected pressures for a blast normal to it, or to shear and smaller lateral pressures for a blast parallel with it. Openings would decrease the duration of lateral pressures but would reduce both the shearing and bending strength of the wall. Under such conditions the best solution is to make all wall elements uniform in width between openings.

If blast enters a house through openings, interior walls may also be exposed to large pressures. If they have a structural

*Uniform Building Code by Pacific Coast Building Officials Conference.

**The increased safe distance is necessary primarily because of the greater spread of pressure at increased height.

†See "Design of Blast Resistant Construction for Atomic Explosions" by C. S. Whitney, B. G. Anderson, and E. Cohen, ACI *Proceedings*, Vol. 51, page 607, Fig. A1.5.

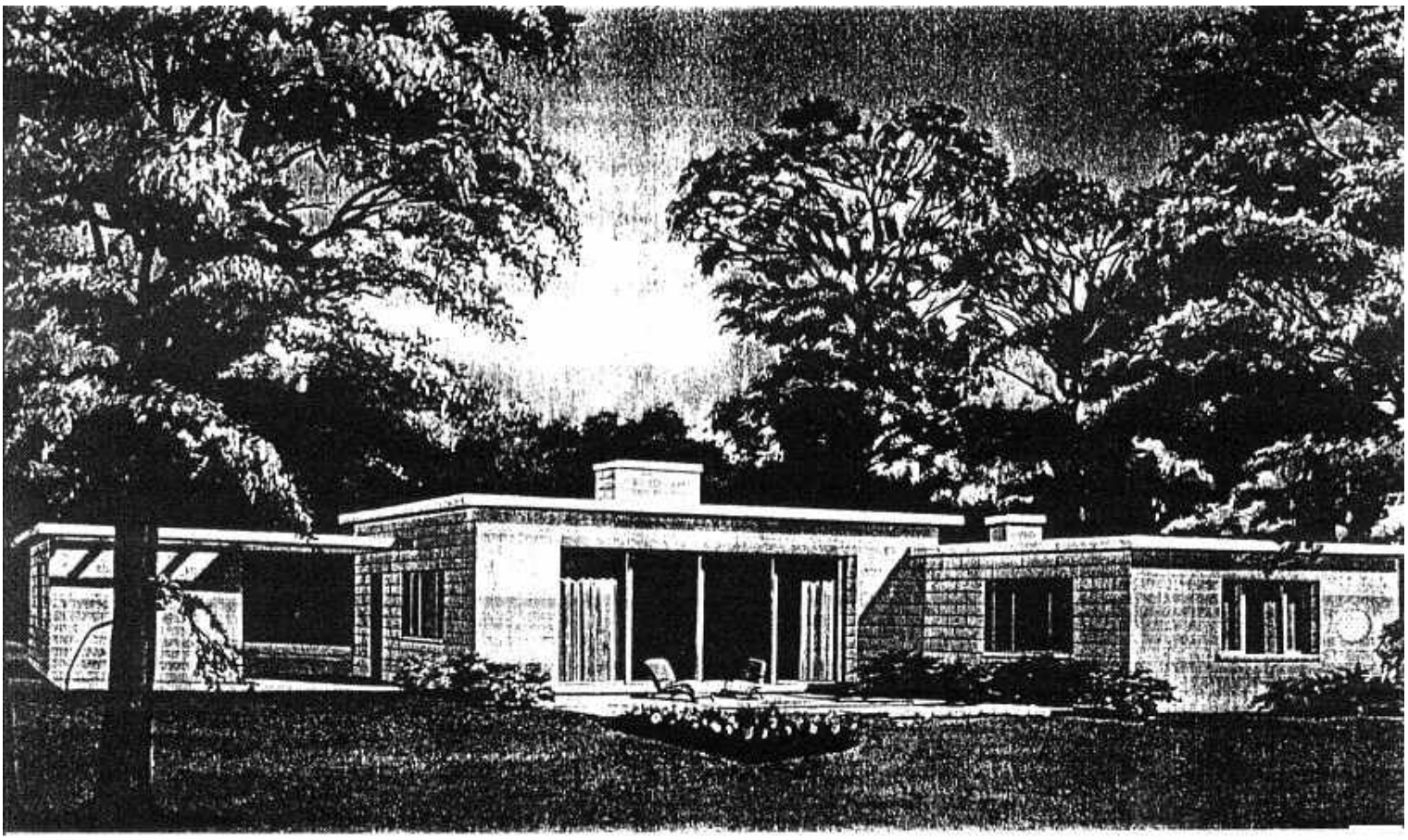

Fig. 10. One-story blast-resistant house

function, they should be designed and built in a manner similar to exterior walls. To limit the maximum unbroken wall area for interior walls is even more important than for exterior walls, since no escape of reflected pressure is possible at roof level.

It is generally advisable to provide approximately the same amount of structural walls in each direction of a building. For illustration, a long, narrow building normally should have longitudinal walls broken up by large windows and have only small openings in transverse walls. The center of gravity of the resistance from all shear walls should coincide as closely as possible with the center of gravity of the total load, in order to avoid twisting of the building. In some cases a rigid concrete frame around a large opening may be necessary for additional strength.

If the house has many openings, the roof will get only a relatively small unbalanced load. It is not desirable, in general, to let the blast reach the basement. Therefore, the floor slab for average conditions would have to be designed for approximately full side-on pressure. If the basement is to be used as a shelter, that portion of the floor over the shelter should be designed for even higher pressures.

Special consideration should be given to layouts that may trap the blast inside the building. This condition would exist, for example, where three solid walls form a U with the open side against the blast. High reflected pressures may occur in such cases against not only the walls but also the floor and roof. The resulting net upward pressure could result in uplift of the roof if it were not properly tied down.

Details of a Blast-Resistant House

Important blast-resistant features are incorporated in the design details of a one-story modern house with basement as shown in Figs. 10, 11 and 12. This house was designed to resist blast at 9,000 ft. from a nominal bomb exploded 2,000 ft. above ground, with the assumption that there is no relief as a result of pressures entering the windows. Because of the large window openings, the house will actually withstand larger pressures than those calculated. No restrictions are imposed on orientation.

The exterior walls of heights suitable for conventional one-story houses are of 12-in. concrete masonry, as shown in Fig. 11. Concealed behind the furring are vertical tierods—No. 7 bars at 24-in. spacing—securely anchored to the roof and the floor. As the wall bends under lateral pressure, it is compressed between the two slabs, which are restrained from moving apart by the tierods (see Fig. 13). The wall acts as a vertical beam with fixed ends subject to an axial load and supported at the roof and floor level. It is capable of resisting pressure from either direction.

The 6-in. reinforced concrete roof slab is designed to withstand the vertical side-on pressures; it also acts as a deep horizontal girder that transmits horizontal reactions from the front wall to the side walls. The advantage of a flat roof is

twofold: (1) by decreasing the height of the building it reduces the total area exposed to reflected pressure; (2) with a strong, flat concrete roof the walls exposed to blast act as beams supported both top and bottom, whereas without such roof construction, the walls would act as cantilevers and have much less resistance.

Side walls act as shear walls that resist the horizontal reactions from the roof. For this reason, as shown in Fig. 12, ample bracing has been provided by walls in both directions.

The 6-in. reinforced concrete floor slab is able to withstand a blast pressure of 360 psi. A shelter area is provided in the basement for protection of the occupants. In that portion of the floor over the shelter, the slab thickness and the reinforcement remain the same, but the span is reduced to approximately 3 ft., which makes the slab safe for a blast pressure of 1,900 psi.

Blast resistance of a windowless house can be predicted accurately by means of a dynamic analysis. Windows complicate the design because they reduce the duration of the load on walls facing the blast. The following equation can be used to estimate the increase in blast resistance of the 12-in. wall when provided with windows and openings spaced not more than 18 ft. and not less than 2 ft. apart:

$$d_s = 350\ (9 + b),$$

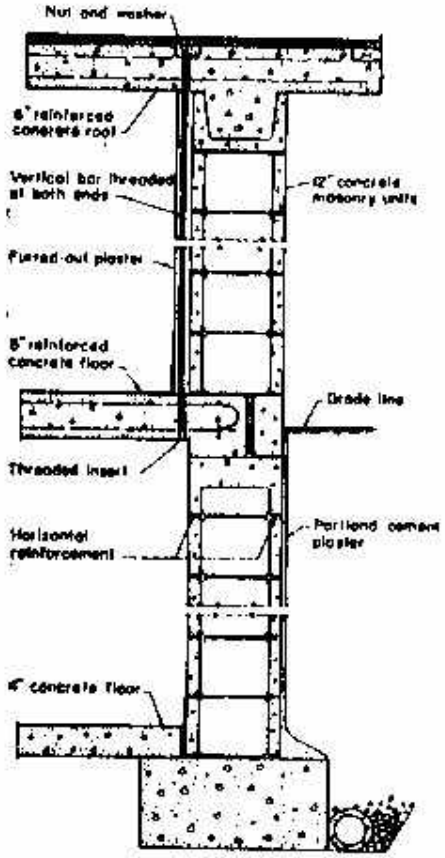

Fig. 11. Details of a reinforced concrete masonry wall.

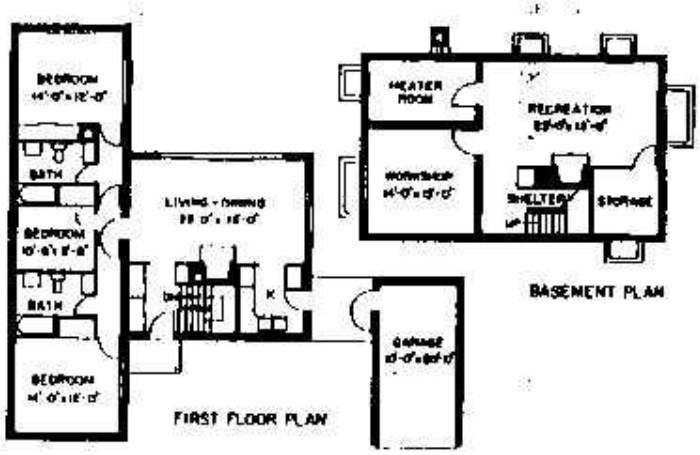

Fig. 12. Floor plans for a one-story blast-resistant house.

where d_s is the safe distance in feet from ground zero and b is the width in feet between adjacent openings.

For a windowless structure the maximum value of $b = 18$ ft. should be used. The formula then gives d_s equal to 9,450 ft. If the relief obtained by windows is taken into account and a 6-ft. width of wall between openings is assumed, minimum safe distance for the front wall is

$$d_s = 350\ (9 + 6) = 5{,}250 \text{ ft.}$$

For an 8-in. concrete masonry wall, the pressure that can be resisted is reduced in proportion to its thickness. For example, the peak side-on pressure for a 12-in. concrete masonry wall without openings at the safe distance of 9,450 ft. is, from Fig. 3, 2.5 psi. An 8 in. wall can therefore resist a peak side-on pressure of $2.5 \times \frac{8}{12} = 1.65$ psi, which is the pressure at a distance of 11,000 ft. Therefore, an 8-in. wall at 11,000 ft. will withstand the same blast that a 12-in. wall will resist at 9,450 ft.

To estimate the blast resistance of the concrete masonry test house at Yucca Flat, referred to on page 5, assume that a 12-in. wall has a width between openings of 5 ft. The minimum safe distance is

$$d_s = 350\ (9 + 5) = 4{,}900 \text{ ft.}$$

At this distance the peak side-on pressure is 7.8 psi for a nominal bomb at 2,000-ft. altitude. For an 8-in. wall this value is reduced to $7.8 \times \frac{8}{12} = 5.20$ psi, which corresponds to a safe distance from ground zero of 6,400 ft. This compares favorably with the value given on page 5, which was calculated by converting the side-on pressure for the actual bomb size and height of explosion used in the test to that of a nominal bomb exploded at 2,000 ft. above ground.

Design Aids

The two load charts, Figs. 14 and 15, may be used to design roof and floor slabs. They give the thickness and reinforcement for a reinforced concrete slab for different spans at various distances from ground zero of a 20-KT bomb. The

height of explosion is assumed to be 2,000 ft. The values in the charts are obtained from a dynamic analysis and the slab deflection is limited to 1/90 of the span. Generally accepted simplifications, as presented in Fig. 7, were made in regard to the pressure-time relationship.

In Fig. 14 relief is not included from pressures entering the building or from turbulence over the edge of the front wall. Therefore, it is applicable to slabs over basements, to side walls parallel to the direction of blast, and to roof slabs on closed buildings. For the relatively long duration of the peak load on which this chart is based, there is little difference between the results of the dynamic and static analyses made of the slabs.

Fig. 15 applies to the special case of a roof slab on a closed building that has a width-to-height ratio and a width-to-depth ratio greater than 3 and that is subject to blast normal to the width of building. The roof spans in the direction of the blast. Except for the extreme ends of the roof, which are designed from the values in Fig. 14, the turbulence over the edge of the front wall reduces the duration of the peak load and permits a less conservative design. The shorter duration in loading permits the static load capacity of the slabs to be from 50 to 75 per cent of the static capacity corresponding to the peak load. This chart will also give approximate results for roofs on partly open buildings that have relieving effects as a result of pressures on the inside.

If slabs are continuous over two or more spans, the effective span length, L_1, may be taken as the distance between points of contraflexure. The same amount of reinforcement as that shown in the charts should also be provided as negative steel

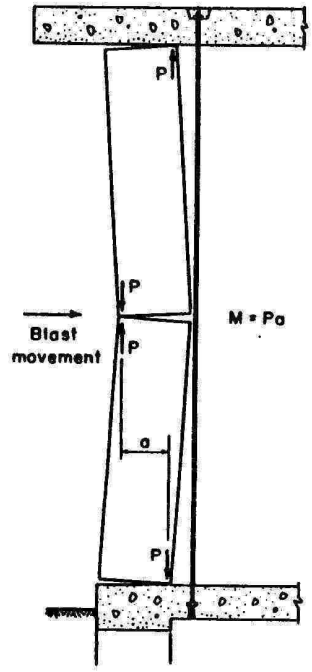

Fig. 13. The effect of an anchored tierod behind a concrete masonry wall.

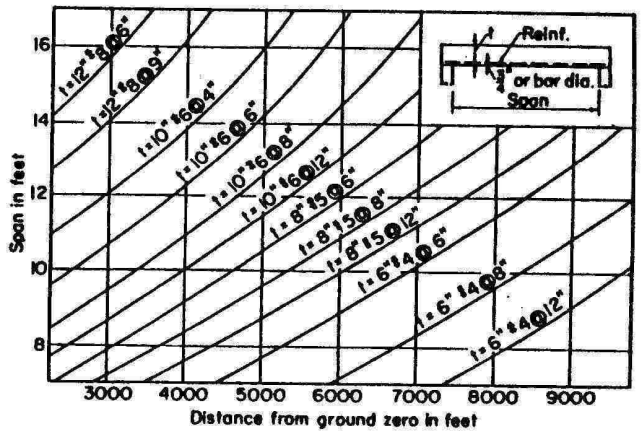

Fig. 14. Design of a simply supported one-way slab for long-duration peak loads from a 20-KT bomb.

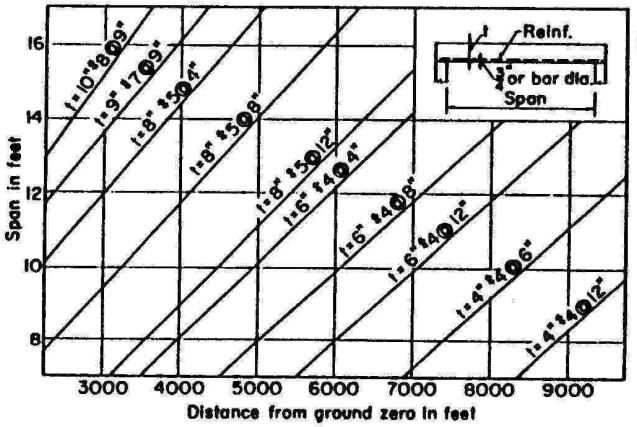

Fig. 15. Design of a simply supported one-way slab for short-duration peak loads from a 20-KT bomb.

over the interior supports. The distance from a point of contraflexure to an adjacent support may be estimated as follows:

At a discontinuous edge	0
At the interior support	
in an exterior bay	$L/4$
In all interior bays	$L/5$

where L is the clear span.

For illustration, a continuous roof slab over two 20-ft. bays will have an effective span, $L_1 = 20(1-1/4) = 15$ ft. If the structure is located 6,000 ft. from ground zero, Fig. 14 shows that the required slab thickness is 10 in., reinforced with No. 6 bars at 6-in. spacing both at midspan and over the interior support. This structure will resist a blast load from a 200-KT bomb at a distance of $d = 6{,}000\sqrt[3]{\frac{200}{20}} = 13{,}000$ ft.

Blast resistance of a one-story house is more a matter of layout and detailing than of structural design. For this reason, only the most simplified design considerations have been given. For larger and more complex structures a detailed dynamic analysis is required.

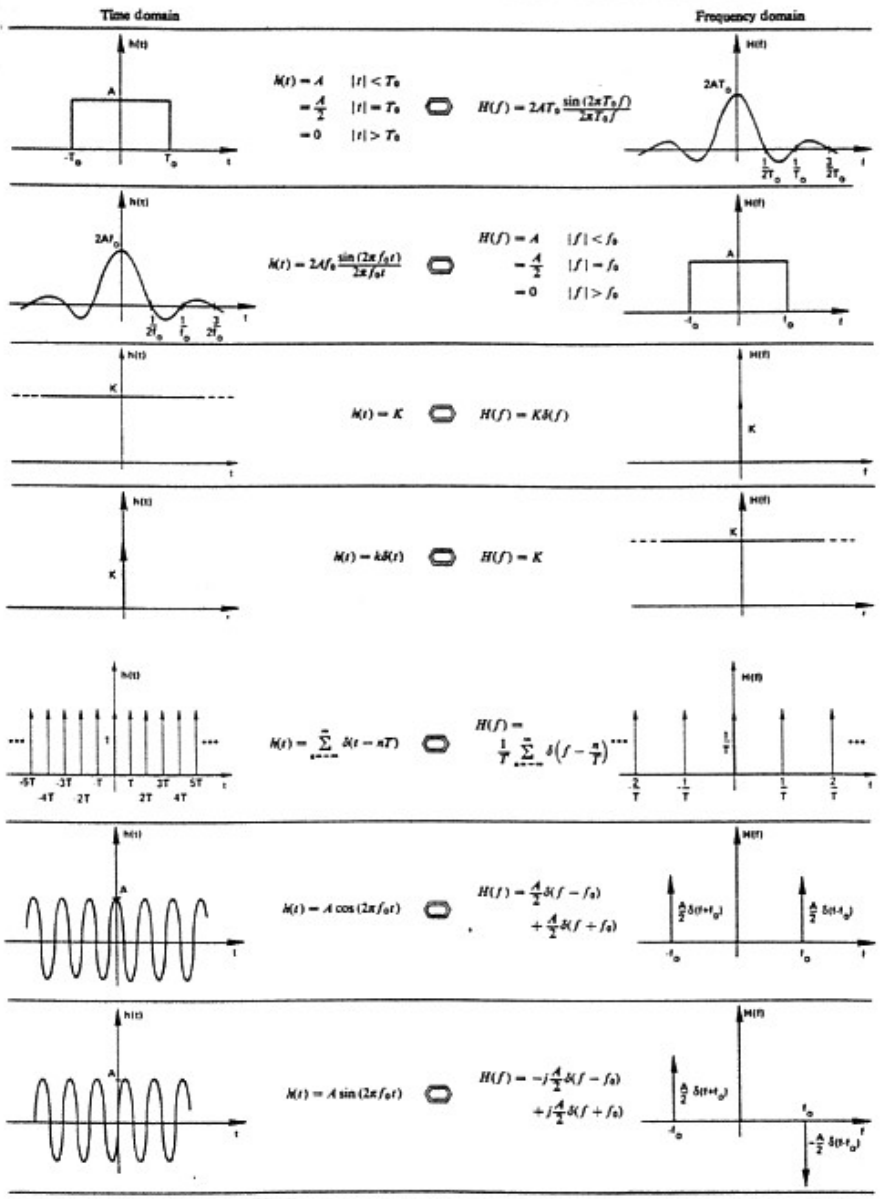

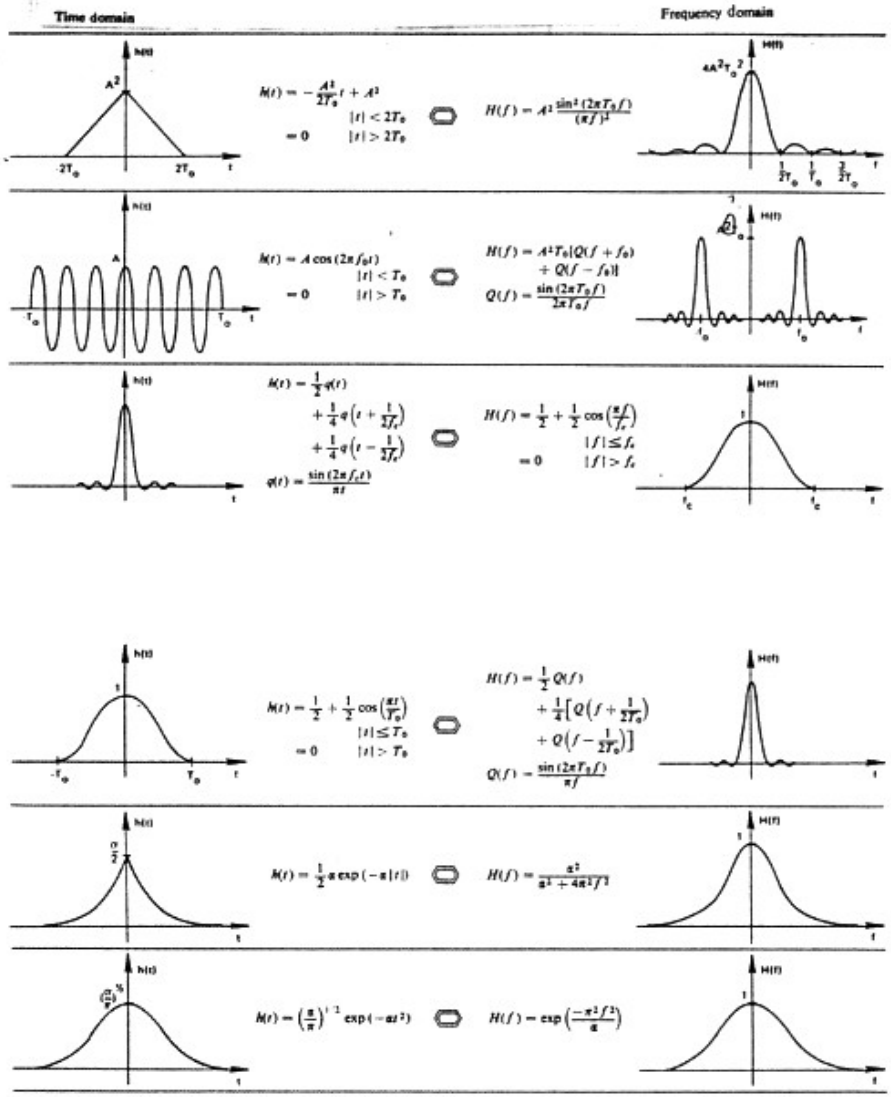

(Brigham, 1974)

Par de Tranformada de Fourier

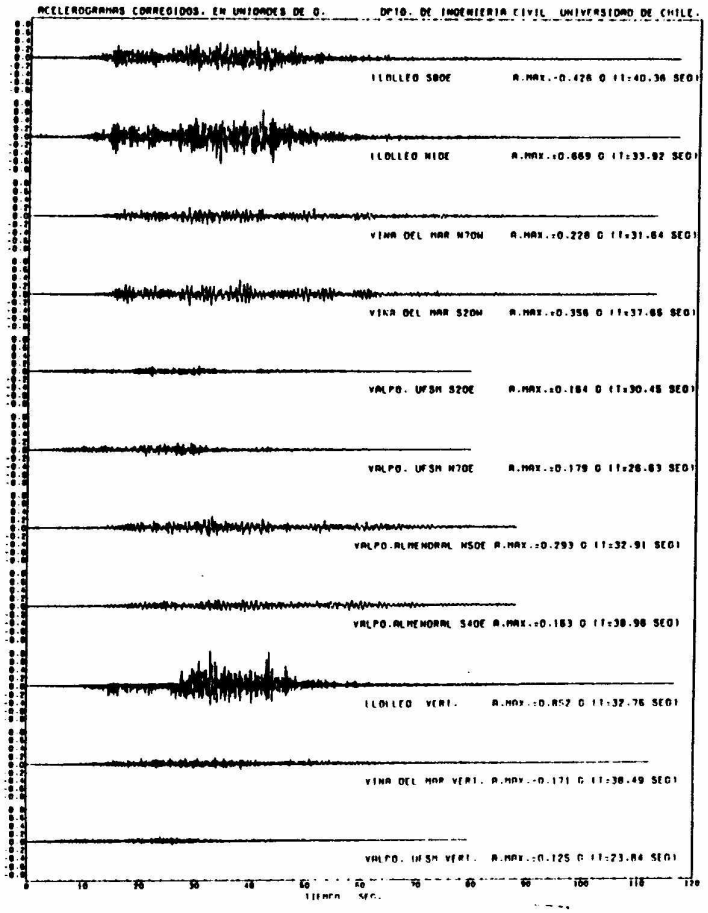

Fig. 3.5. Sismo del 3 de Marzo de 1985. M_s = 7.8. Registros de aceleración.

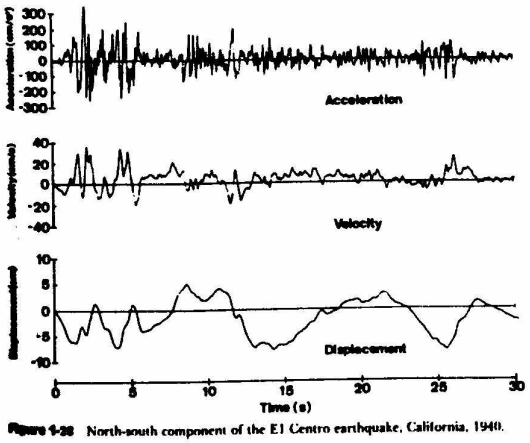

Figure 1-26 North-south component of the El Centro earthquake, California, 1940.

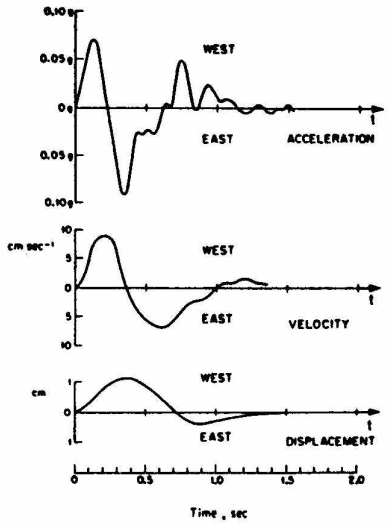

Figure 1-27 East-west component of the Port Hueneme earthquake, 1957. [*From G. W. Housner and D. E. Hudson, The Port Hueneme earthquake of March 18, 1957*, Bull. Seismol. Soc. Am., *48(2), 163–168 (1958).*]

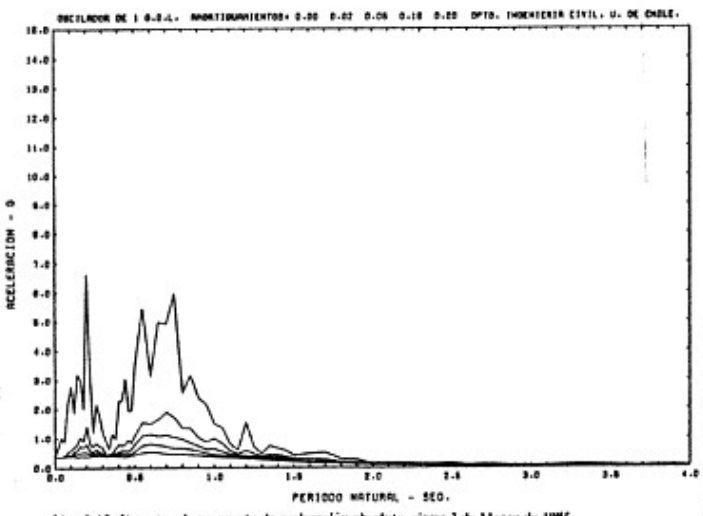

Fig. 3.12. Espectro de respuesta de aceleración absoluta, sismo 3 de Marzo de 1985. Viña del Mar S20W.

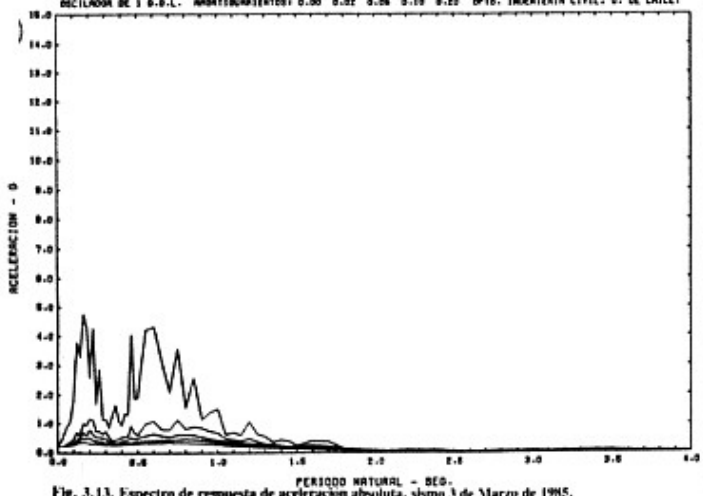

Fig. 3.13. Espectro de respuesta de aceleración absoluta, sismo 3 de Marzo de 1985. Viña del Mar N70W.

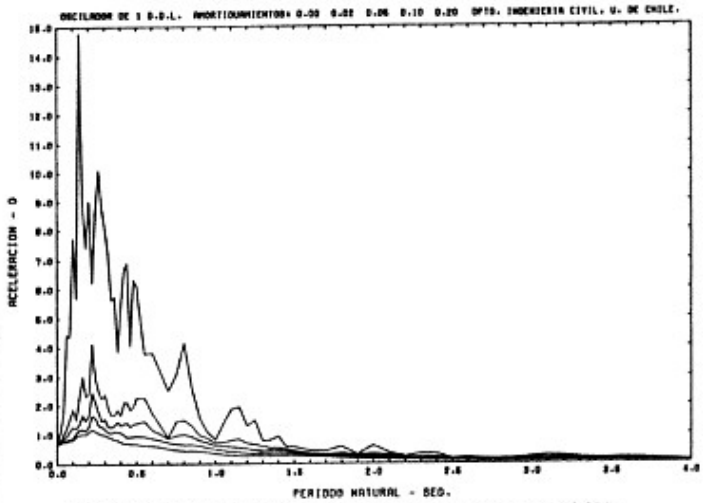

Fig. 3.10. Espectro de respuesta de aceleración absoluta, sismo 3 de Marzo de 1985. Llolleo N10E.

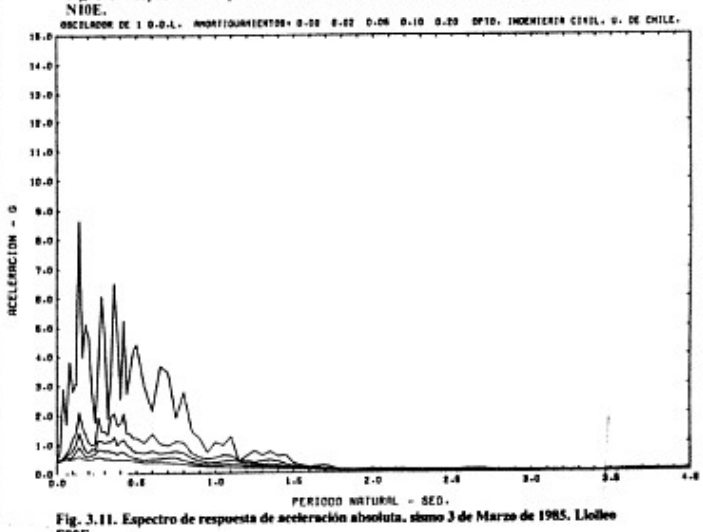

Fig. 3.11. Espectro de respuesta de aceleración absoluta, sismo 3 de Marzo de 1985. Llolleo S80E.

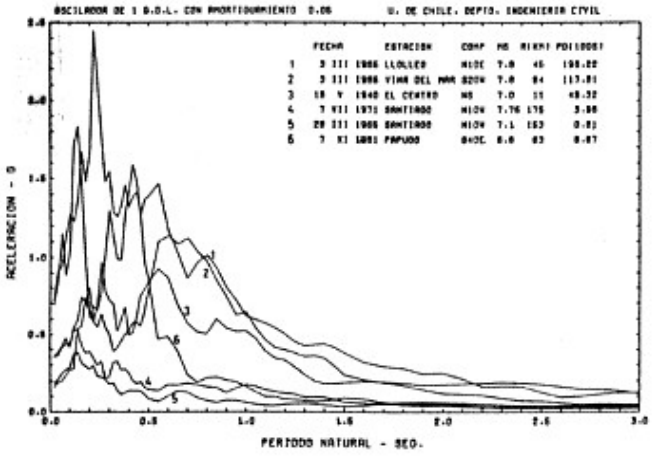

Fig. 3.18 Comparación de los espectros de respuesta de aceleración absoluta. Sismo 3 de Marzo de 1985. Llolleo N10E y Viña del Mar S20W. Con otros recopilados.

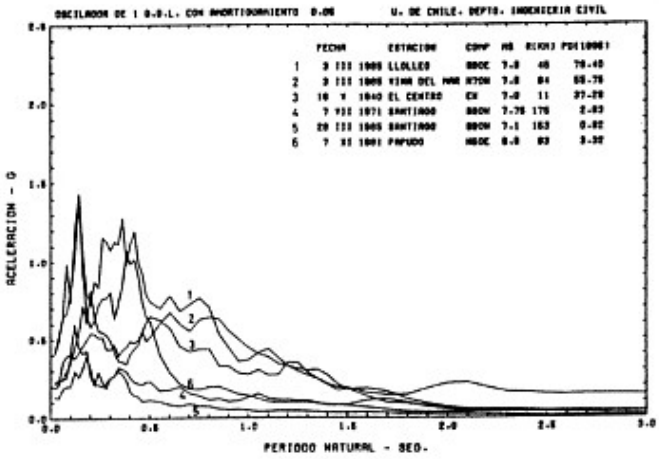

Fig. 3.19. Comparación de los espectros de respuesta de aceleración absoluta. Sismo 3 de Marzo de 1985. Llolleo S80E y Viña del Mar N70W. Con otros recopilados.

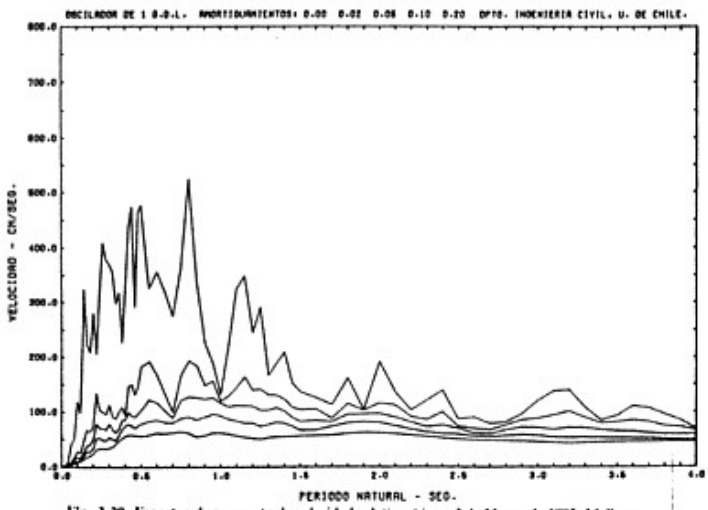

Fig. 3.20. Espectro de respuesta de velocidad relativa. Sismo 3 de Marzo de 1985. Llolleo N10E.

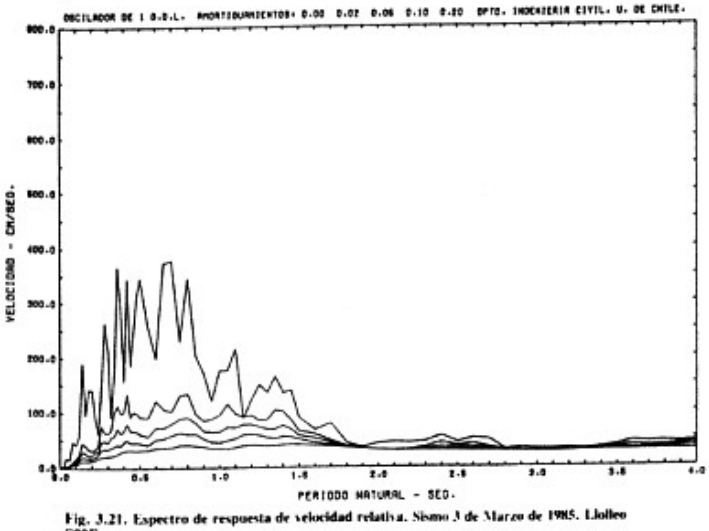

Fig. 3.21. Espectro de respuesta de velocidad relativa. Sismo 3 de Marzo de 1985. Llolleo S80E.

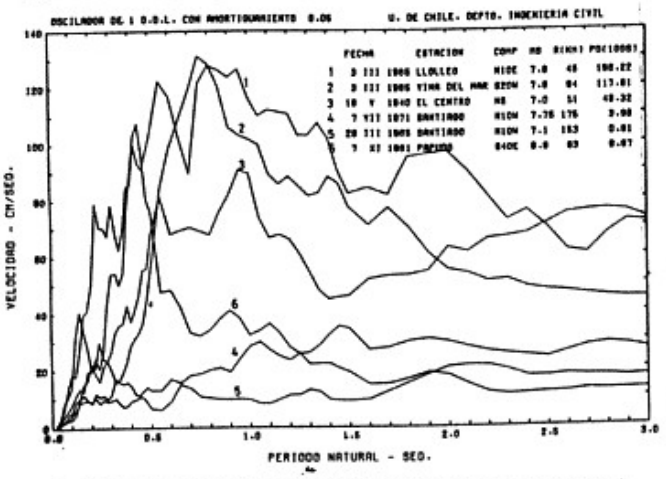

Fig. 3.28. Comparación de los espectros de respuesta de velocidad relativa. Sismo 3 de Marzo de 1985. Llolleo N10E y Viña del Mar S20W, con otros recopilados.

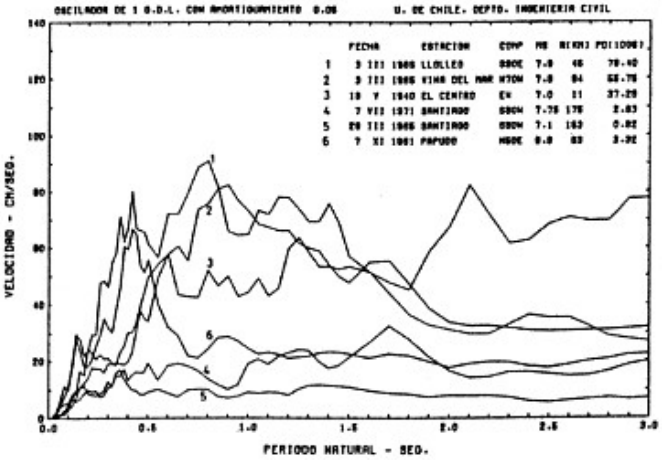

Fig. 3.29. Comparación de los espectros de respuesta de velocidad relativa. Sismo 3 de Marzo de 1985. Llolleo S80E y Viña del Mar N70W, con otros recopilados.

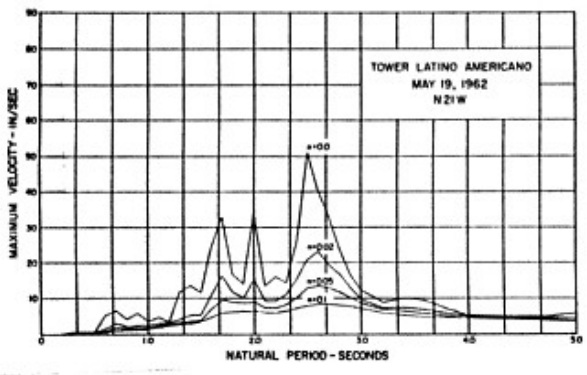

Fig. 4.17. Velocity response spectrum S_v of the N21W component of the ground acceleration recorded in Mexico City, May 19, 1962. The epicenter of this magnitude 7 shock was 200 mi south of the city. The accelerograph was in the basement of a 43-story building in the center of town, on the old lake bed.

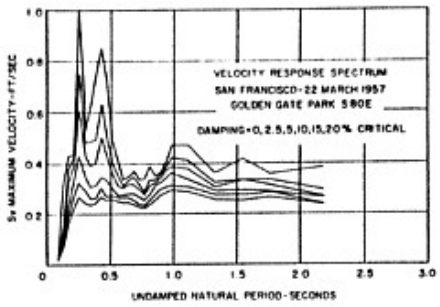

Fig. 4.18. Velocity response spectrum S_v of the S80E component of ground acceleration recorded in Golden Gate Park, San Francisco, March 22, 1957. The epicenter of this magnitude 5.3 shock was 8 mi south of the accelerograph.

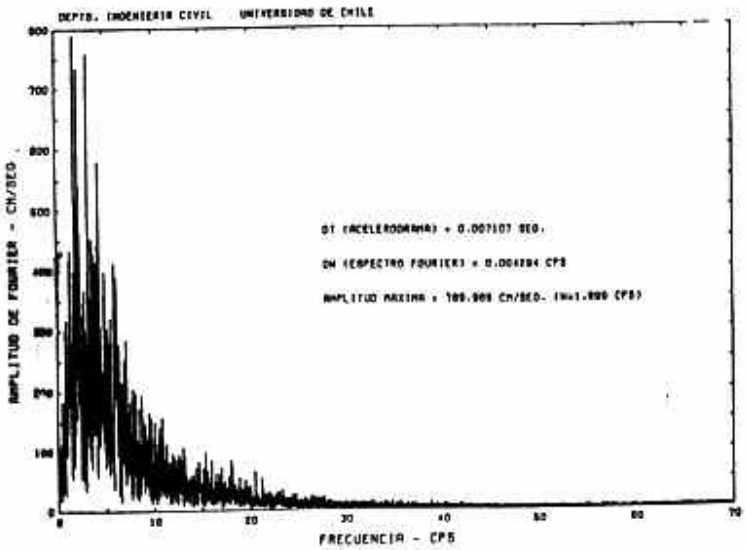

Fig. 3.30. Espectro de amplitud de Fourier de Aceleración. Sismo 3 de Marzo de 1985. Llolleo N10W.

Fig. 4.9. Fourier spectrum of ground acceleration component S69E recorded at Taft, California, July 21, 1952. The Fourier spectrum (dotted line) is similar to the zero-damped, velocity-response spectrum (solid line).

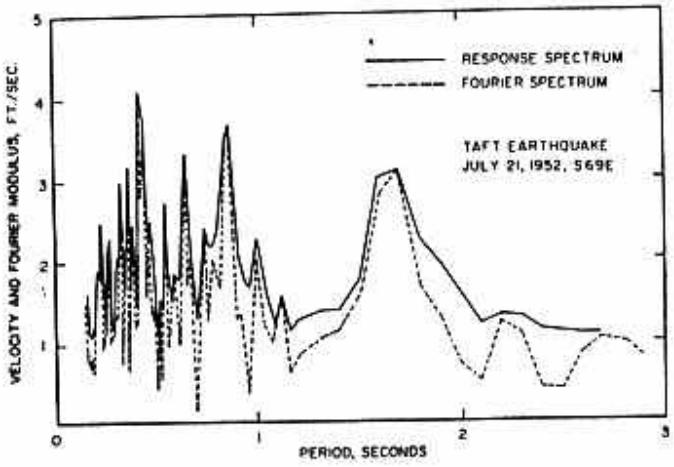

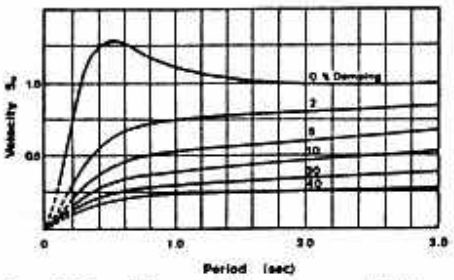

Figure 2-10 Smoothed average velocity response spectra S_v by Housner; arbitrary scale. [*G. W. Housner, Behavior of structures during earthquakes,* J. Eng. Mech. Div., Am. Soc. Civ. Eng., *85(EM-4), 109–129 (1959).*]

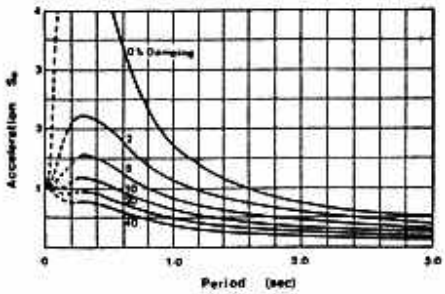

Figure 2-11 Smoothed average acceleration response spectra S_a by Housner; arbitrary scale. [*G. W. Housner, Behavior of structures during earthquakes,* J. Eng. Mech. Div., Am. Soc. Civ. Eng., *85(EM-4), 109–129 (1959).*]

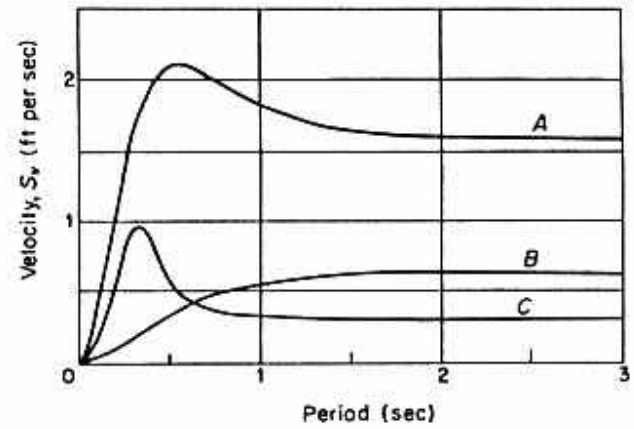

Fig. 4.18. Idealized undamped velocity spectrum curves that illustrate the effect of magnitude and distance. Curve *A*, 25 mi from center of large earthquake; curve *B*, 70 mi from center of large shock; curve *C*, 8 mi from center of small ($M = 5.3$) shock.

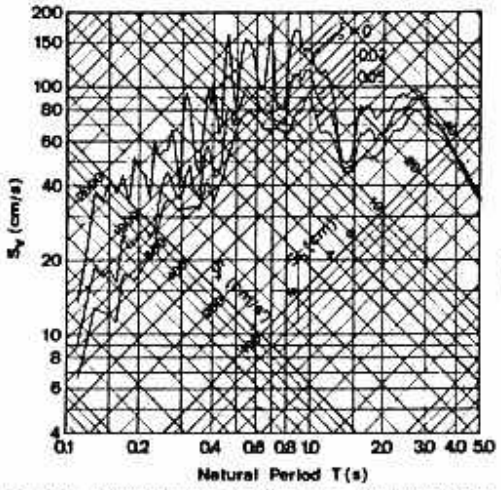

Figure 2-14 Response spectra derived from north-south component of the El Centro earthquake, California, 1940.

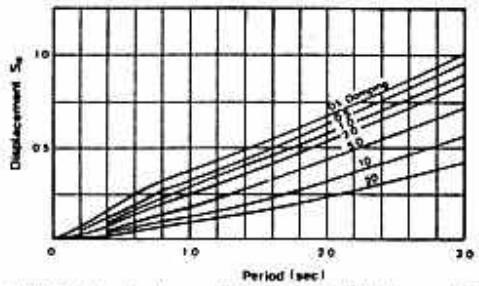

Figure 2-12 Smoothed average displacement spectra S_d by Housner; arbitrary scale. [*G. W. Housner, Strong ground motion in* R. L. Wiegel (ed.), Earthquake Engineering, *Prentice-Hall, Inc., Englewood Cliffs, N.J., 1970, 75–91.*]

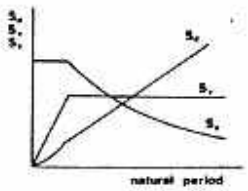

Figure 2-13 General shapes of response spectra.

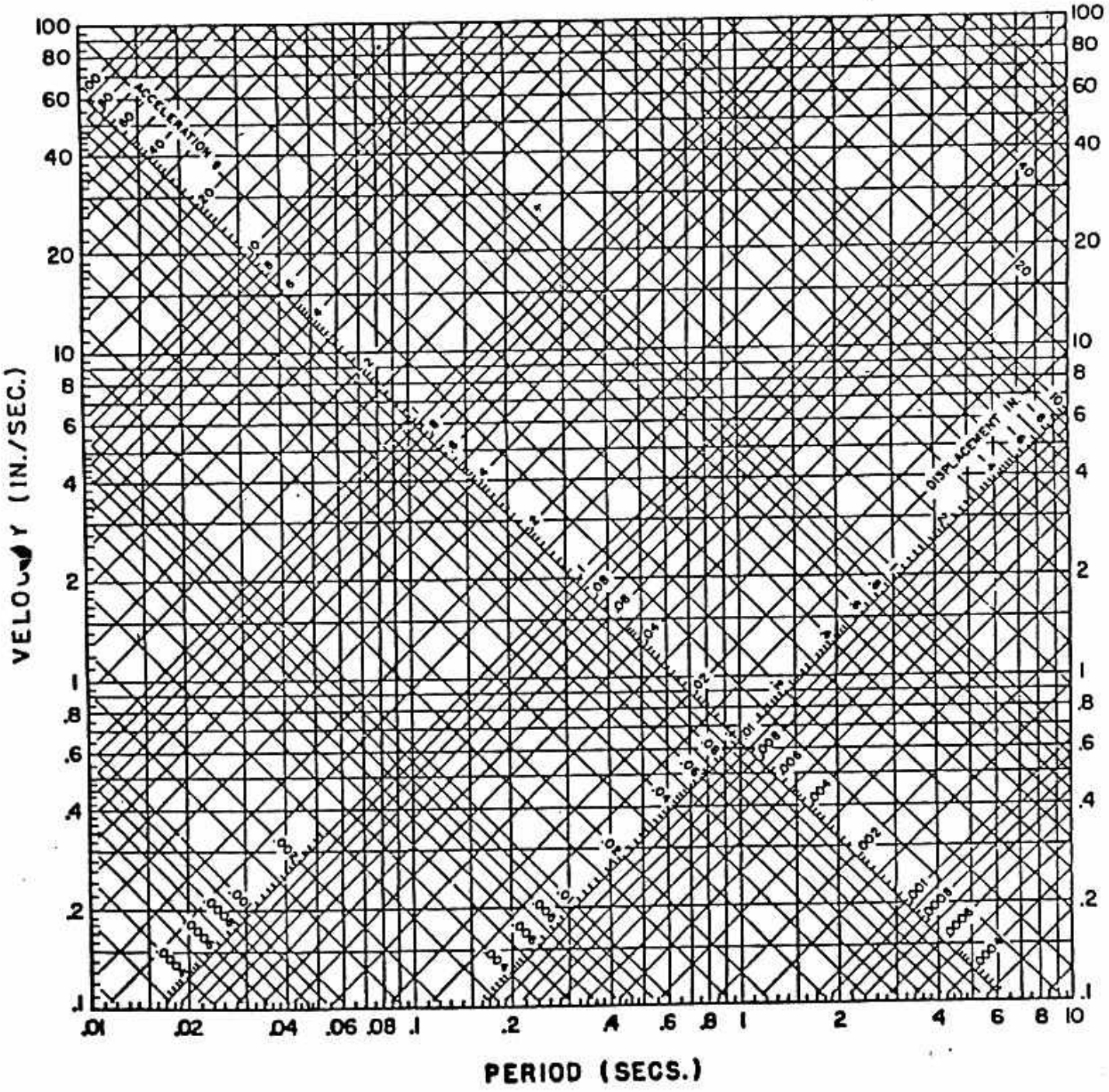

FIG. 3.23.- FOUR WAY LOG.-PAPER

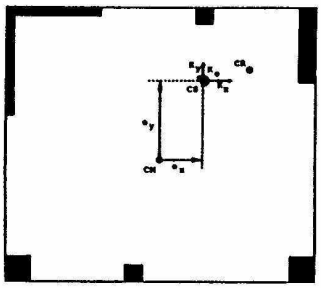

Figure 2.1: One story plan definitions.

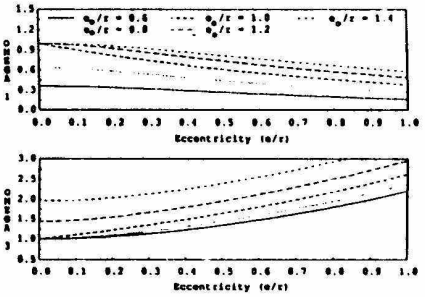

Figure 2.2: Ratio of coupled to uncoupled frequencies as a function of $(e_x/r)^2$ and $(e/r)^2$.

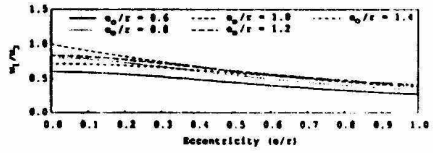

Figure 2.3: Ratio of coupled frequencies as a function of $(e_x/r)^2$ and $(e/r)^2$.

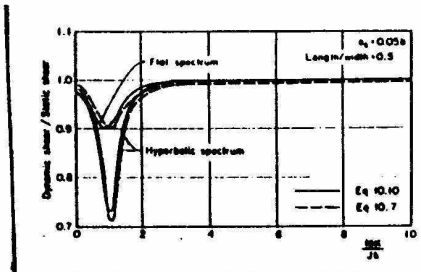

Figure 10.9. Relation between the dynamic and static shears
After Rosenblueth and Elorduy (1969a).

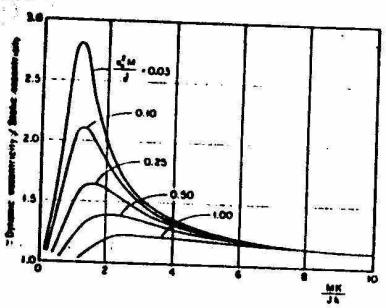

Figure 10.10. Magnification factor for eccentricity.
After Rosenblueth and Elorduy (1969a).

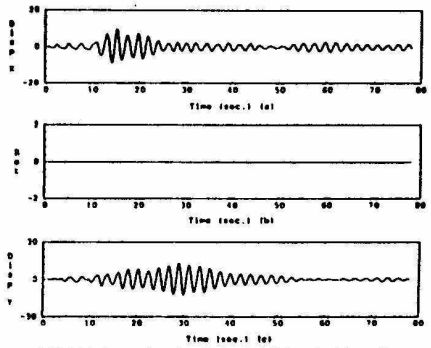

Figure 2.12: Model D. Viscous damping 5% of critical. Bidirectional input. From 1966 Mt. Lewis earthquake at CSMIP station 57357.

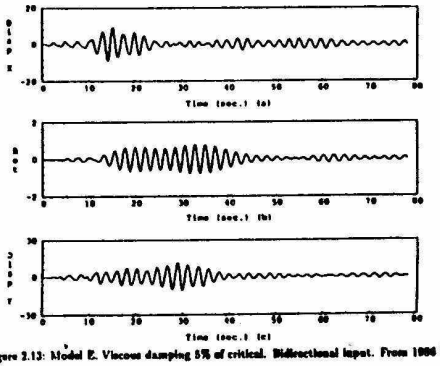

Figure 2.13: Model E. Viscous damping 5% of critical. Bidirectional input. From 1966 Mt. Lewis earthquake at CSMIP station 57357.

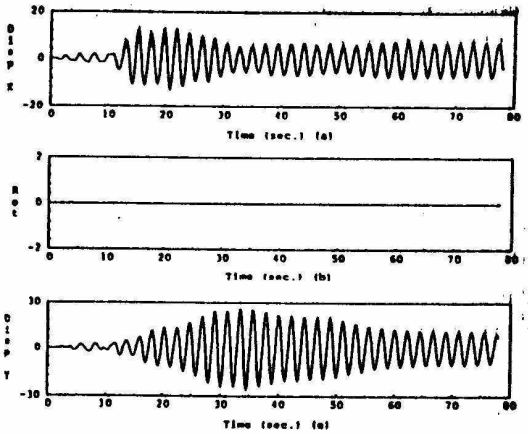

Figure 2.10: Model D. Viscous damping 1% of critical. Bidirectional input. From 1966 Mt. Lewis earthquake at CSMIP station 57357.

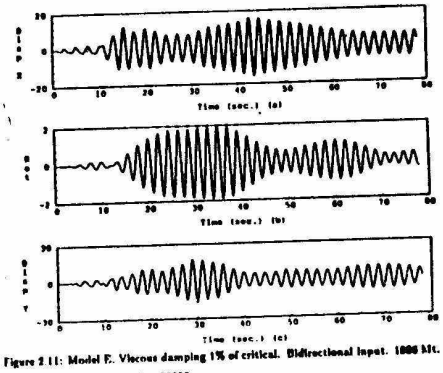

Figure 2.11: Model E. Viscous damping 1% of critical. Bidirectional input. 1966 Mt. Lewis earthquake at CSMIP station 57357.

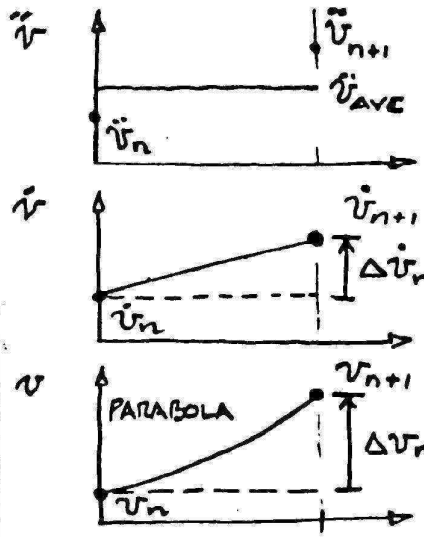

SINGLE STEP METHOD BASED ON CONSTANT "AVERAGE" ACCELERATION

EQUILIBRIUM COMPUTED AT $t=(n+1)\Delta t$

KNOWS: $m; C; K; v_n; \dot{v}_n; \ddot{v}_n$

$$\Delta\ddot{v}_n = \ddot{v}_{n+1} - \ddot{v}_n \qquad \text{I a}$$

$$\ddot{v}_{AVE} = \ddot{v}_n + \frac{\Delta\ddot{v}_n}{2} \qquad \text{I b}$$

FOR VELOCITY:

$$\dot{v}_{n+1} = \dot{v}_n + \Delta\dot{v}_n \qquad \text{II a}$$

$$\Delta\dot{v}_n = \Delta t\,\ddot{v}_{AVE} = \ddot{v}_n \Delta t + \frac{\Delta t}{2}\Delta\ddot{v}_n \qquad \text{II b}$$

FOR DISPLACEMENT:

$$v_{n+1} = v_n + \Delta v_n \qquad \text{III a}$$

$$\Delta v_n = \frac{1}{2}\Delta t\,\Delta\dot{v}_n + \Delta t\,\dot{v}_n \qquad \text{III b}$$

OR

$$\Delta v_n = \frac{\Delta t^2}{2}\ddot{v}_n + \frac{\Delta t^2}{4}\Delta\ddot{v}_n + \Delta t\,\dot{v}_n \qquad \text{III c}$$

TO GET $\ddot{v}_{n+1}$ IN TERMS OF v_{n+1} (SOLVING EQ. III c)

$$\Delta\ddot{v}_n = \frac{4}{\Delta t^2}\left(\Delta v_n - \frac{1}{2}\ddot{v}_n\Delta t^2 - \dot{v}_n\Delta t\right) = \frac{4}{\Delta t^2}\Delta v_n - \frac{4}{\Delta t}\dot{v}_n - 2\ddot{v}_n \qquad \text{IV (a)}$$

USING EQS I(a) and III(a)

$$\ddot{v}_{n+1} = \ddot{v}_n + \Delta\ddot{v}_n = \frac{4}{\Delta t^2}\Delta v_n - \frac{4}{\Delta t}\dot{v}_n - \ddot{v}_n = \frac{4}{\Delta t^2}\left(v_{n+1} - v_n\right) - \frac{4}{\Delta t}\dot{v}_n - \ddot{v}_n \qquad \text{IV (b)}$$

TO GET $\dot{v}_{n+1}$ IN TERMS OF v_{n+1} (SOLVING EQ III(b))

$$\Delta\dot{v}_n = \frac{2}{\Delta t}\left(\Delta v_n - \dot{v}_n\Delta t\right) = \frac{2}{\Delta t}\Delta v_n - 2\dot{v}_n \qquad \text{V(a)}$$

USING EQS. II a and III a

$$\dot{v}_{n+1} = \dot{v}_n + \Delta v_n = \frac{2}{\Delta t}\Delta v_n - \dot{v}_n = \frac{2}{\Delta t}\left(v_{n+1} - v_n\right) - \dot{v}_n \qquad \text{V(b)}$$

SUBSTITUTING III b and V b in EQUATIONS OF MOTION ($m\ddot{v} + C\dot{v} + Kv = P$)

$$m\left(\frac{4}{\Delta t^2}\left(v_{n+1} - v_n\right) - \frac{4}{\Delta t}\dot{v}_n - \ddot{v}_n\right) + C\left(\frac{2}{\Delta t}\left(v_{n+1} - v_n\right) - \dot{v}_n\right) + K v_{n+1} = P_{n+1}$$

COLLECTING TERMS RELATED TO v_{n+1}

$$\left(\frac{4}{\Delta t^2}m + \frac{2}{\Delta t}C + K\right)v_{n+1} = P_{n+1} + m\left(\frac{4}{\Delta t^2}v_n + \frac{4}{\Delta t}\dot{v}_n + \ddot{v}_n\right) + C\left(\frac{2}{\Delta t}v_n + \dot{v}_n\right) \qquad \text{VI}$$

SO $v_{n+1} = \tilde{K}^{-1}\tilde{P}_{n+1}$ WHERE: $\tilde{K} = \frac{4}{\Delta t^2}m + \frac{2}{\Delta t}C + K$

$$\tilde{P}_{n+1} = P_{n+1} + m\left(\frac{4}{\Delta t^2}v_n + \frac{4}{\Delta t}\dot{v}_n + \ddot{v}_n\right) + C\left(\frac{2}{\Delta t}v_n + \dot{v}_n\right)$$

PROCESS: GIVEN $n, v_n, \dot{v}_n, \ddot{v}_n, P_{n+1}, m, c, k$

1. COMPUTE $\tilde{K}$
2. COMPUTE $\tilde{P}$
3. SOLVE $v_{n+1} = \tilde{K}^{-1}\tilde{P}_{n+1}$
4. $\dot{v}_{n+1} = \frac{2}{\Delta t}(v_{n+1} - v_n) - \dot{v}_n$ (FROM EQ. IV b)
5. $\ddot{v}_{n+1} = \frac{4}{\Delta t^2}(v_{n+1} - v_n) - \frac{4}{\Delta t}\dot{v}_n - \ddot{v}_n$ (from EQ. IV b)

   OR

   $\ddot{v}_{n+1} = \frac{P_{n+1} - C\dot{v}_{n+1} - Kv_{n+1}}{m}$ (by equilibrium).
6. $n = n+1$ GO TO STEP (1)

ALTERNATIVE FORMULATION

FOR $m\Delta\ddot{v} + C\Delta\dot{v} + K\Delta v = \Delta P$ $\qquad \Delta P_n = P_{n+1} - P_n$

SUBSTITUTING EQS. IIIa and IIa

$$m\left(\frac{4}{\Delta t^2}\Delta v_n - \frac{4}{\Delta t}\dot{v}_n - 2\ddot{v}_n\right) + C\left(\frac{2}{\Delta t}\Delta v_n - 2\dot{v}_n\right) + K\Delta v_n = \Delta P_n$$

COLLECTING TERMS RELATED TO Δv_n

$$\left(\frac{4}{\Delta t^2}m + \frac{2}{\Delta t}C + K\right)\Delta v_n = \Delta P + m\left(\frac{4}{\Delta t}\dot{v}_n + 2\ddot{v}_n\right) + 2C\dot{v}_n$$

OR

$$\Delta v_n = \hat{K}^{-1}\Delta\hat{P}_n \quad \text{where} \quad \hat{K} = \frac{4}{\Delta t^2}m + \frac{2}{\Delta t}C + K$$

$$\Delta\hat{P}_n = \Delta P_n + m\left(\frac{4}{\Delta t}\dot{v}_n + 2\ddot{v}_n\right) + 2C\dot{v}_n$$

PROCESS: GIVEN $n, v_n, \ddot{v}_n, \dot{v}_n; \Delta P_n = P_{n+1} - P_n; m, C, K$

1. COMPUTE $\hat{K}$
2. COMPUTE $\hat{P}$
3. SOLVE $\Delta v_n = \hat{K}^{-1}\Delta P_n$
4. $v_{n+1} = v_n + \Delta v_n$
5. $\Delta\dot{v}_n = \frac{2}{\Delta t}\Delta v_n - 2\dot{v}_n$

   $\dot{v}_{n+1} = \dot{v}_n + \Delta\dot{v}_n$
6. $\Delta\ddot{v}_n = \frac{4}{\Delta t^2}\Delta v_n - \frac{4}{\Delta t}\dot{v}_n - 2\ddot{v}_n$

   $\ddot{v}_{n+1} = \ddot{v}_n + \Delta\ddot{v}_n$

   OR $\ddot{v}_{n+1} = \frac{P_{n+1} - C\dot{v}_{n+1} - Kv_{n+1}}{m}$
7. GO TO 1

NOTES:
- METHOD IS SELF STARTING.
- METHOD IS UNCONDITIONALLY STABLE
- FOR ACCURACY USE $\Delta t < \frac{T}{10}$
- FOR NONLINEAR SYSTEMS USE ALTERNATIVE METHOD AND SUBSTITUTE:
  - K_T for K in $K\Delta v$ TERMS
  - R for Kv IN GLOBAL EQUILIBRIUM EQUATION

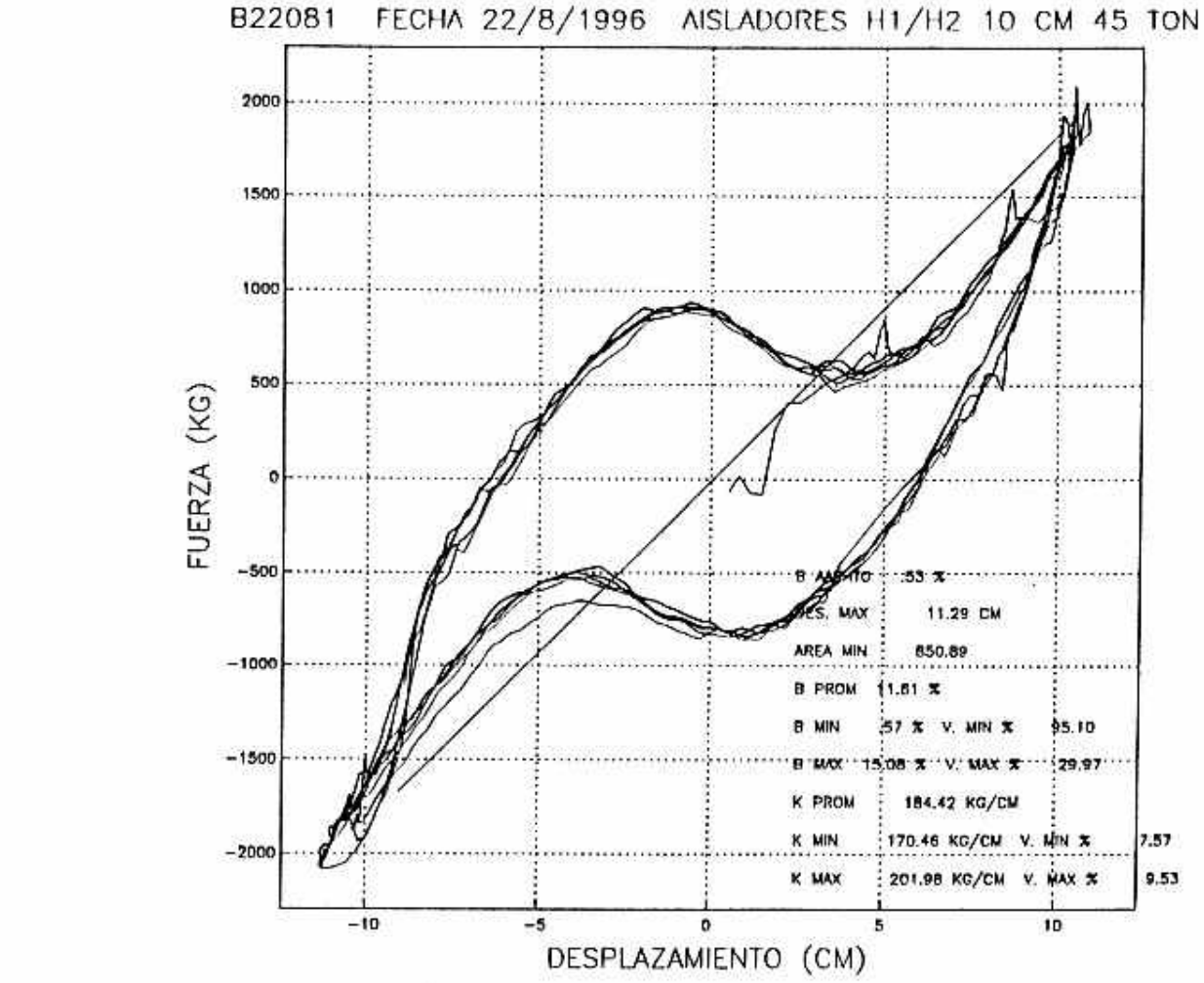
B22081 FECHA 22/8/1996 AISLADORES H1/H2 10 CM 45 TON
FUERZA (KG)
DESPLAZAMIENTO (CM)
2000
1500
1000
500
0
-500
-1000
-1500
-2000
-10
-5
0
5
10
B AMORTIG .53 %
DES. MAX 11.29 CM
AREA MIN 650.89
B PROM 11.61 %
B MIN .57 % V. MIN % 95.10
B MAX 15.08 % V. MAX % 29.97
K PROM 184.42 KG/CM
K MIN 170.46 KG/CM V. MIN % 7.57
K MAX 201.98 KG/CM V. MAX % 9.53

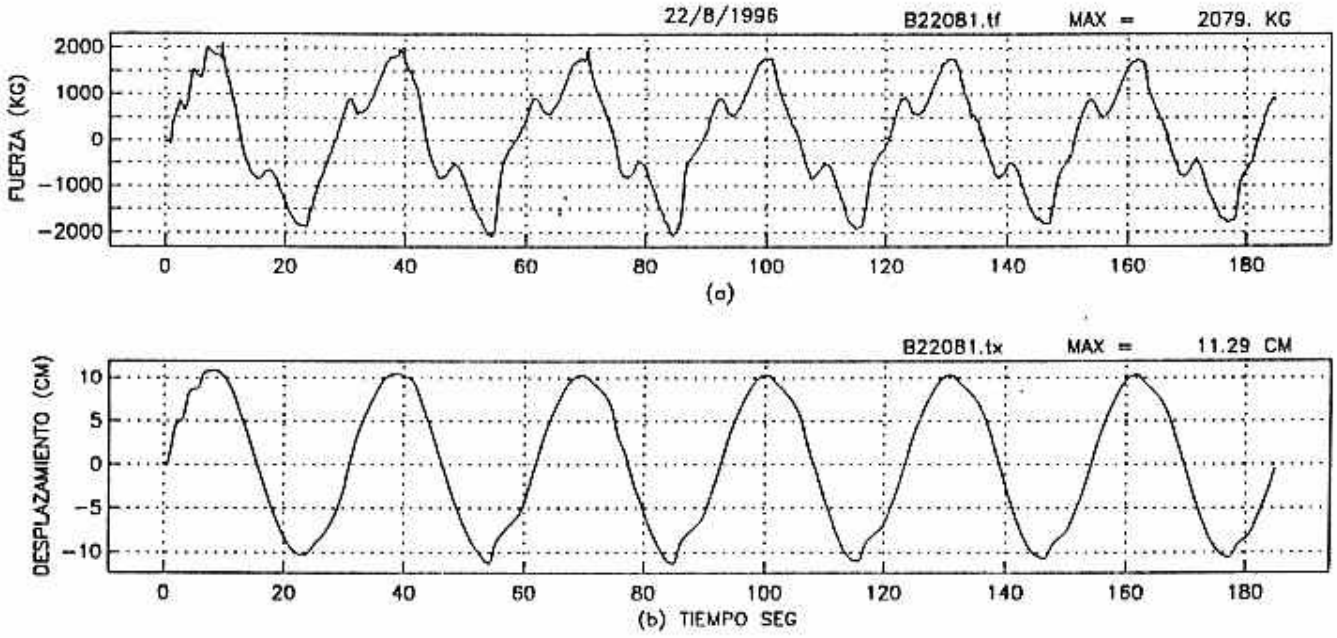
22/8/1996
B22081.tf
MAX = 2079. KG
FUERZA (KG)
2000
1000
0
-1000
-2000
0
20
40
60
80
100
120
140
160
180
(a)
B22081.tx
MAX = 11.29 CM
DESPLAZAMIENTO (CM)
10
5
0
-5
-10
0
20
40
60
80
100
120
140
160
180
(b) TIEMPO SEG

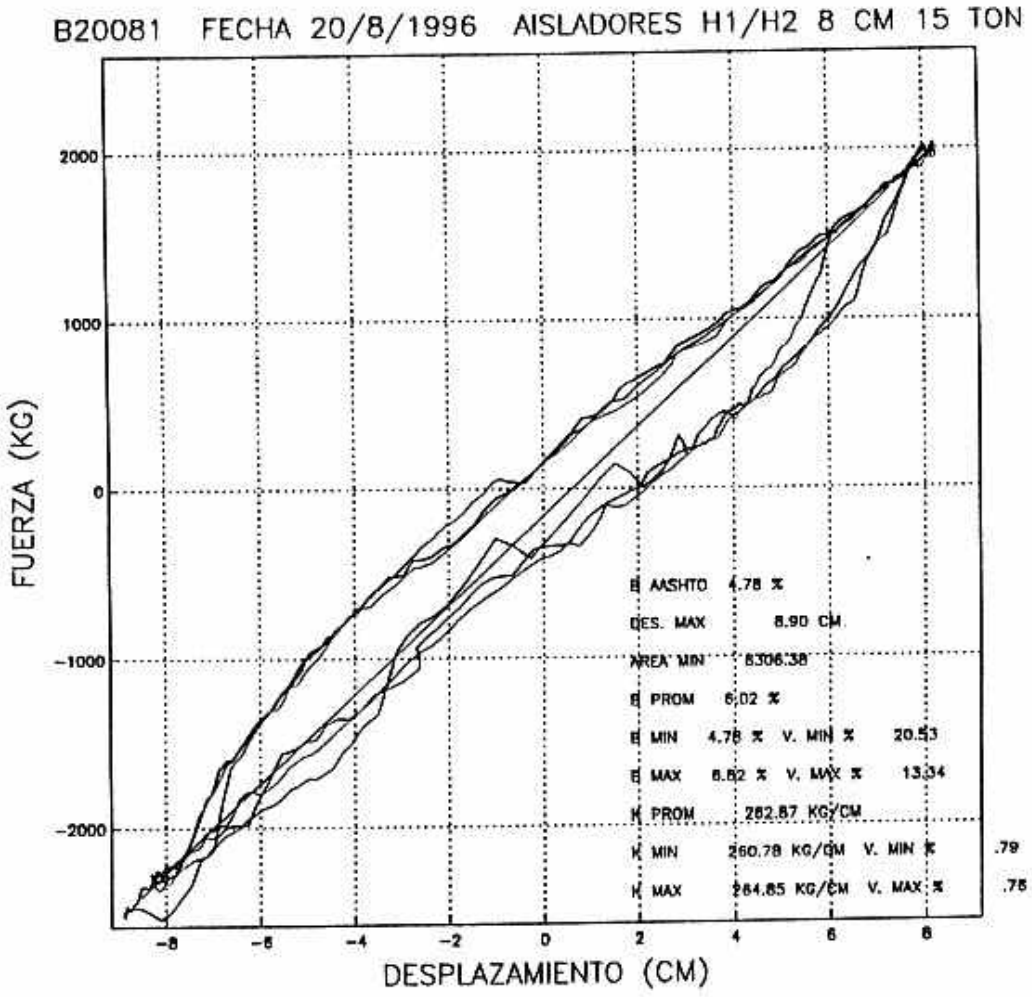
B20081 FECHA 20/8/1996 AISLADORES H1/H2 8 CM 15 TON
FUERZA (KG)
DESPLAZAMIENTO (CM)
2000
1000
0
-1000
-2000
-8
-6
-4
-2
0
2
4
6
8
E AASHTO 4.78 %
DES. MAX 8.90 CM
AREA MIN 8306.38
E PROM 6.02 %
E MIN 4.78 % V. MIN % 20.53
E MAX 8.62 % V. MAX % 13.34
K PROM 282.87 KG/CM
K MIN 260.78 KG/CM V. MIN %
K MAX 284.85 KG/CM V. MAX %
.79
.75

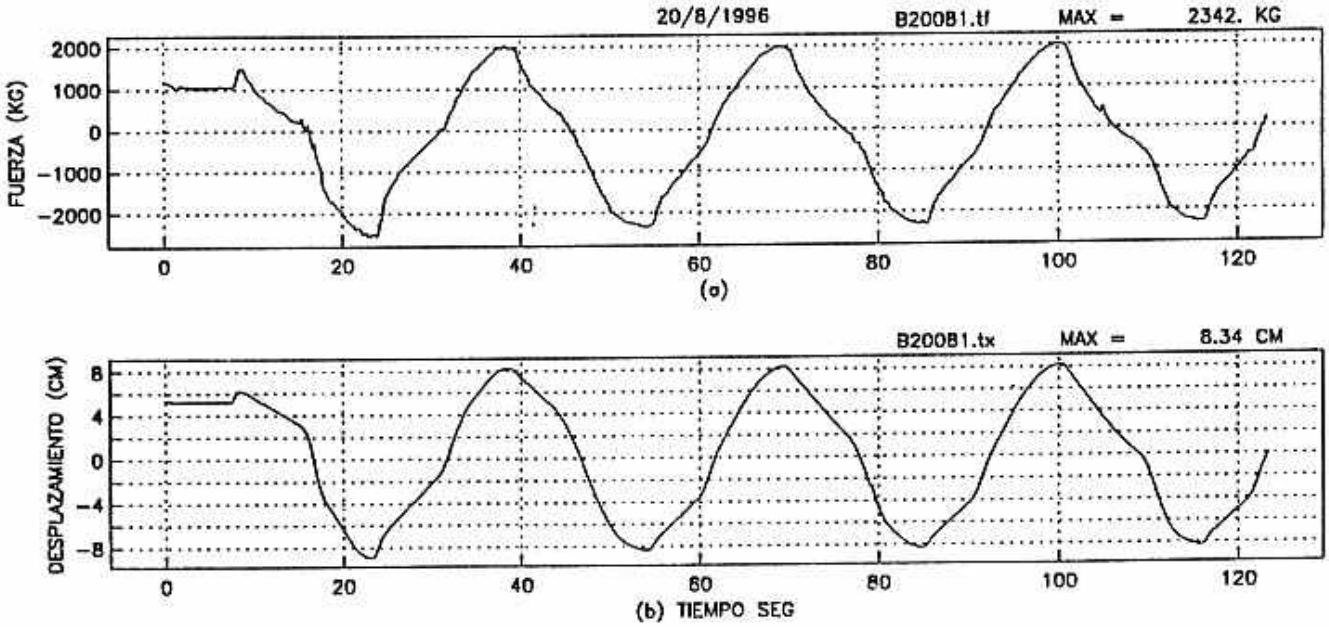
20/8/1996 B20081.tf MAX = 2342. KG
FUERZA (KG)
2000
1000
0
-1000
-2000
0
20
40
60
80
100
120
(a)
B20081.tx MAX = 8.34 CM
DESPLAZAMIENTO (CM)
8
4
0
-4
-8
0
20
40
60
80
100
120
(b) TIEMPO SEG

```
function [d,h]= respcon(m,T,b,vg,Fs)
%
%       [d,h] = respcon(m,T,b,vg,Fs)
%
%       Genera respuesta de un oscilador linear estable
%       con propiedades b y w a  una  senal  de aceleracion vg.
%       Parametros de entrada   m: masa del sistema
%                               b: amortigumiento critico
%               T: periodo no amortiguado del oscilador sec
%               vg: registro de aceleracion
%               Fs:frecuencia de muestreo en registro de aceleracion
%
%               r: respuesta en desplazamiento
%               h: respuesta impulsiva
%       Calcula la respuesta usando convolucion
%
%       Ruben Boroschek 9-9-96
%

[xm,xn]=size(vg);

if  xm > xn
   vg=vg';
   xn=xm;
end
%  longitud de h(t), supone 0.001 de amplitud inicial
% numero de ciclos de periodo
mT=fix(1.099/b)*Fs*T;
if mT > xn
   mT=xn;
end
% frecuencia amortiguada
w=2*pi/T;
wd=w*sqrt(1-b*b);
%  propiedades del instrumento
%  genera respuesta impulsiva del instrumento
h=imp(m,b,wd,mT,Fs);
% calcula respuesta usando convolucion
d=conv(vg,h)/Fs;
d=r(1:xn)';
end
```

```
function h = imp(m,b,w,n,Fs)
%
%       h = imp(m,b,w,n,Fs)
%
%       Genera funcion de impulso para sistema lineal mecanico
%       Parametros de entrada   m: masa del sistema
%                               b: amortigumiento critico
%               w: frecuencia del oscilador rad/sec
%               n: tamano del vector a crear
%               Fs: frecuencia de muestreo
%
%                h(t)=exp(-w*b*t) * sin(wd*t) /[m * wd]
%
%       Ruben Boroschek 9-9-96
%

t=(0:n-1)/Fs;
wd=w*sqrt(1-b*b);
h=exp(-w*b*t).*sin(wd*t)/m/wd;
end
```

```
function [v,hh,vw,beta] = respfre(m,T,b,vg,Fs)
%
%       [v,hh,vw,beta] = respfre(m,T,b,vg,Fs)
%
%       Genera  respuesta de oscilador en el espacio de la frecuencia
%       Parametros de entrada   b: amortigumiento critico
%                               T: periodo del oscilador sec
%                               vg:  senal de entrada
%                               m: masa del oscilador
%                               Fs: frecuencia de muestreo de la senal
%
%                               v: respuesta de desplazamiento
%                               hh: funcion de frecuencia de respuesta
%                               vw: fft de vg
%                               beta: razon de frecuencias para n/2+1
%
%       Ruben Boroschek 9-9-96
%

% longitud vector de entrada
n=length(vg);
% Duracion del registro
Tp=n/Fs;
% paso de Frecuencia
dw=2*pi/Tp;
% frecuencia natural y rigidez
wo=2*pi/T;
k=m*wo*wo;
% senal en el espacio de la frecuencia
vw=fft(vg);
%
[h,beta]=hn(b,k,wo,dw,n/2+1);
hh=zeros(n,1);
h=h';
hh(1:n/2+1)=conj(h);
hh(n/2+2:n)=(h(n/2:-1:2));
v=real(ifft(hh.*vw));
```

```
function [h,beta] = hn(b,k,Fo,dF,n)
%
%       [h,beta] = hn(b,k,Fo,Fs,n) (espectro )
%       [h,beta] = hn(b,k,Fo,F) (valor escalar para F/Fo)
%
%       Genera funcion de impulso en frecuencia para sistema lineal mecanico
%       Parametros de entrada   b : amortigumiento critico
%               Fo: frecuencia del oscilador rad/sec (2 pi Fn)
%               k : rigidez del sistema (si k=1 h(0)=1)
%               Fs: paso de frecuencia (Fs/(2*n))=dF
%               n : tamano del vector a crear
%
%                               beta : relacion de frecuencias F/Fo
%                               h=1/k[1-(F./Fo).^2+j*2*b.*(F./Fo)]
%
%       Ruben Boroschek 1-1-98
%

% Para el caso de valor escalar
F=dF;

% para el caso de espectro
if nargin > 4
   dF=dF/(2*n);
   F=(0:n-1)*dF;
end

beta=F./Fo;
nF=length(F);
unos=ones(1,nF);
h=(unos/k)./(unos-(beta).^2+(j*2*b).*(beta));
```

```
function [x,v,a]=respnewmark(m,T,b,P,Fs,xo,vo,beta,gama)
% [x,v,a]=respnewmark(m,T,b,P,Fs,xo,vo,beta,gama);
% [x,v,a]=respnewmark(-m,k,c,P,Fs,xo,vo,beta,gama);
% Esta funcion proporciona la respuesta de un sistema con rigidez y amortiguamiento
% lineal por medio del método de Newmark.
% PARAMETROS DE ENTRADA:
% m,T,b     : Masa, periodo y razon de amortiguamiento critico del sistema.
% [-]m,k,c  : masa(con signo negativo),rigidez y amortiguamiento del sistema.
% Fs        : Frecuencia de muestreo
% P         :excitacion
% xo,vo     : condicion iniciales def 0
% beta      : 1/2 aceleracion constante; 1/6 (def) aceleracion lineal.
% gama      : 1/2 def opcion amortiguamiento artificial.
% OBSERVACION:
% Para el caso de aceleracion constante en el intervalo se recomienda FS*T<infinito y
% para el caso de aceleracion linealmente creciente se recomienda Fs*T<0.551.
% rbk, pm 19-03-03

if nargin < 6 | isempty(xo)
   xo=0;
end

if nargin < 7 | isempty(vo)
   vo=0;
end

if nargin < 8 | isempty(beta)
   beta=1/6;
end

if nargin < 9 | isempty(gama)
   gama=1/2;
end

% Vectores salida
[P]=fila(P);
x=0*P;
v=x;
a=x;

if m > 0 % Propiedades T y b
   w=2*pi/T;
   k=m*w*w;
   c=2*m*w*b;
else     % Propiedades k c
   k=T;
   c=b;
   m=abs(m);
   w=(sqrt(k/m));
   b=(c/(2*m*w));
end

% CONDICIONES INICIALES Y CONSTANTES
dt=1/Fs;
dt2=dt*dt;
x(1)=xo;
v(1)=vo;
```

```
% Ecuacion de equilibrio paso 1
a(1)=(P(1)-c*v(1)-k*x(1))/m;

% Constantes del metodo.
k1=k+gama*c/(beta*dt)+m/(beta*dt2);
A=m/(beta*dt)+c*gama/beta;
B=m/(2*beta)+dt*(gama/(2*beta)-1)*c;

for i=1:([length(P)]-1)
   deltaP=P(i+1)-P(i)+A*v(i)+B*a(i);
   deltax=deltaP/k1;
   deltav=gama*deltax/(beta*dt)-gama*v(i)/beta+dt*(1-gama/(2*beta))*a(i);
   deltaa=deltax/(beta*dt2)-v(i)/(beta*dt)-a(i)/(2*beta);

   x(i+1)=x(i)+deltax;
   v(i+1)=v(i)+deltav;
   a(i+1)=a(i)+deltaa;
end

x=columna(x);
v=columna(v);
a=columna(a);
```

RESPUESTA IMPULSO

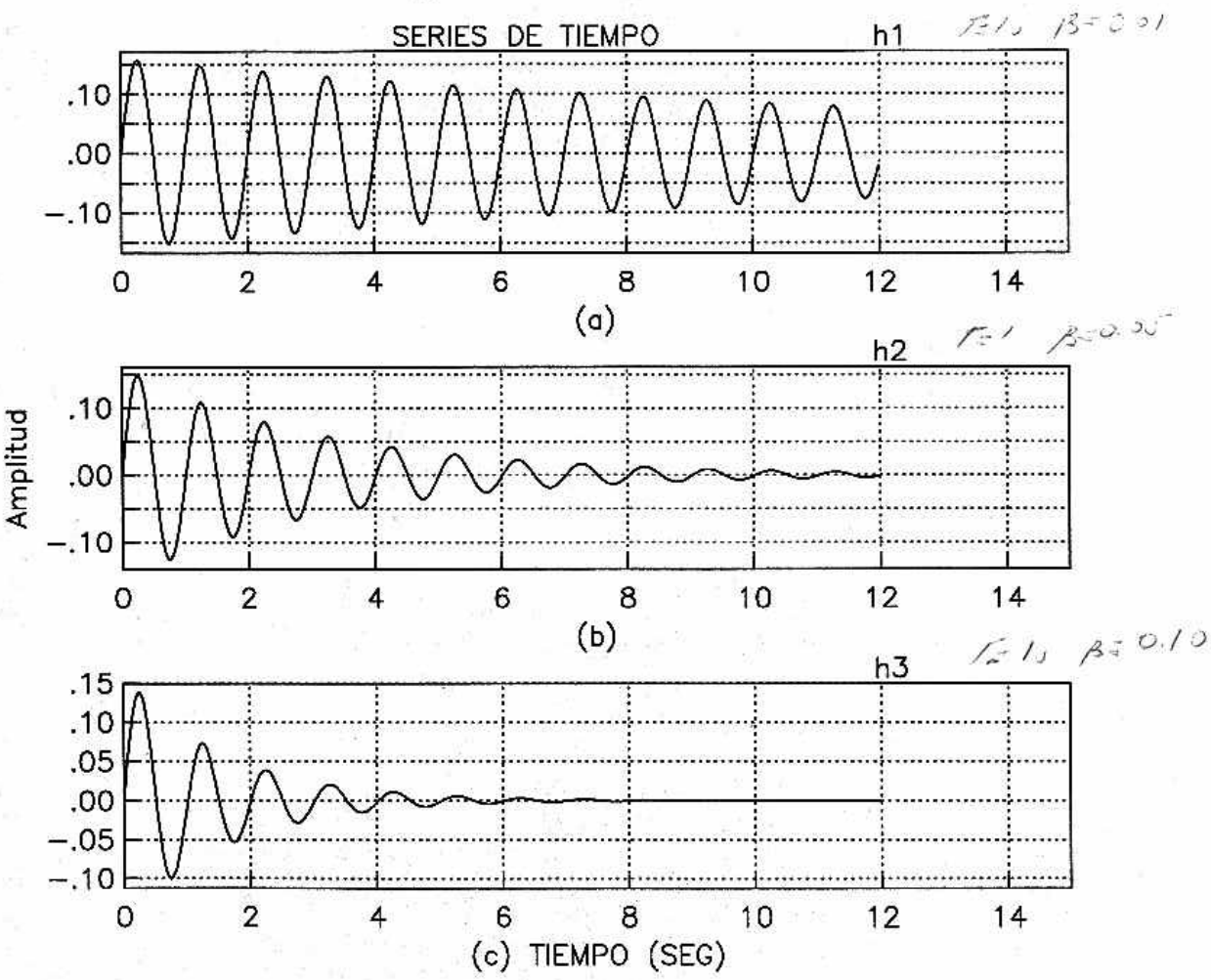

RESPUESTA IMPULSO

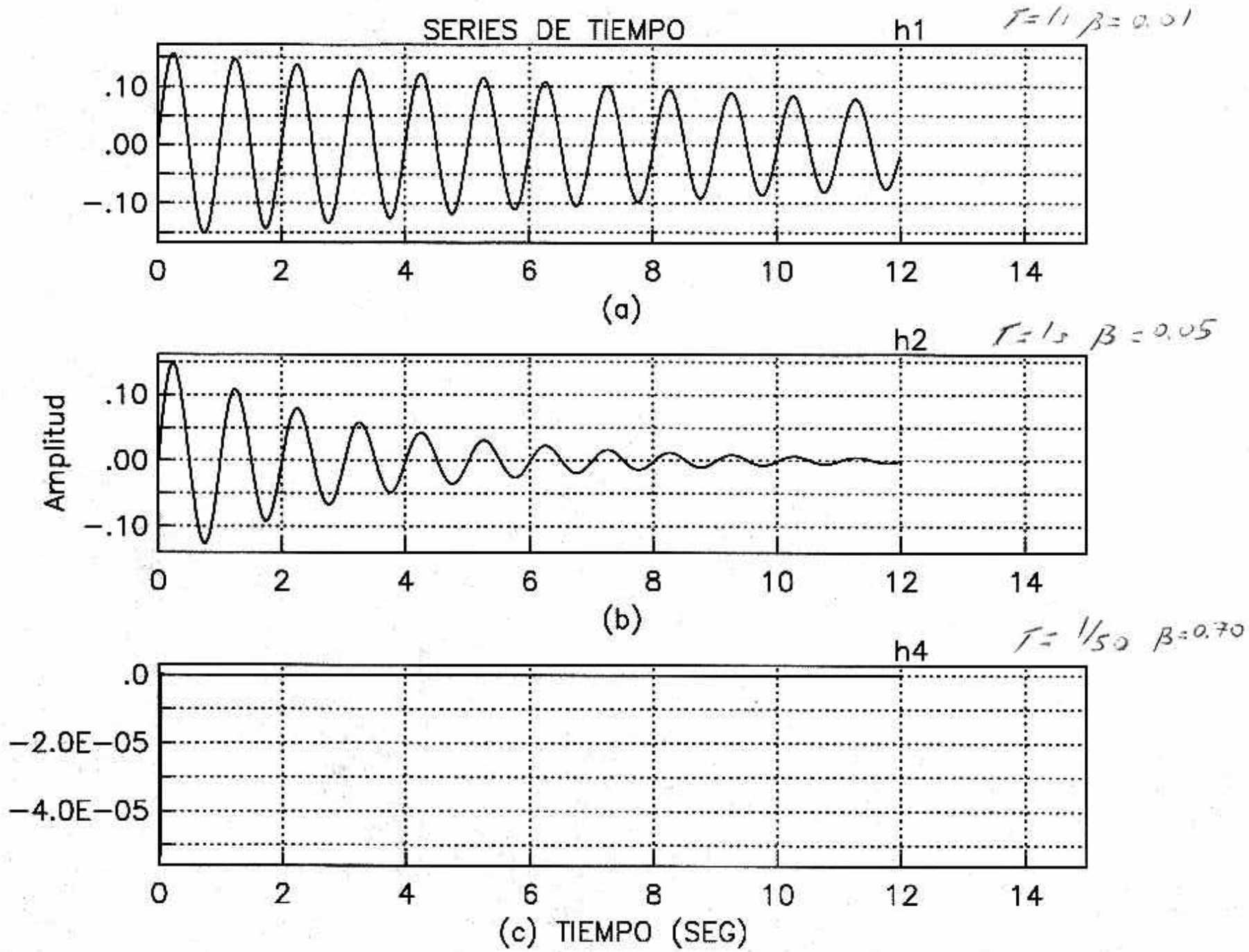

RESPUESTA IMPULSO

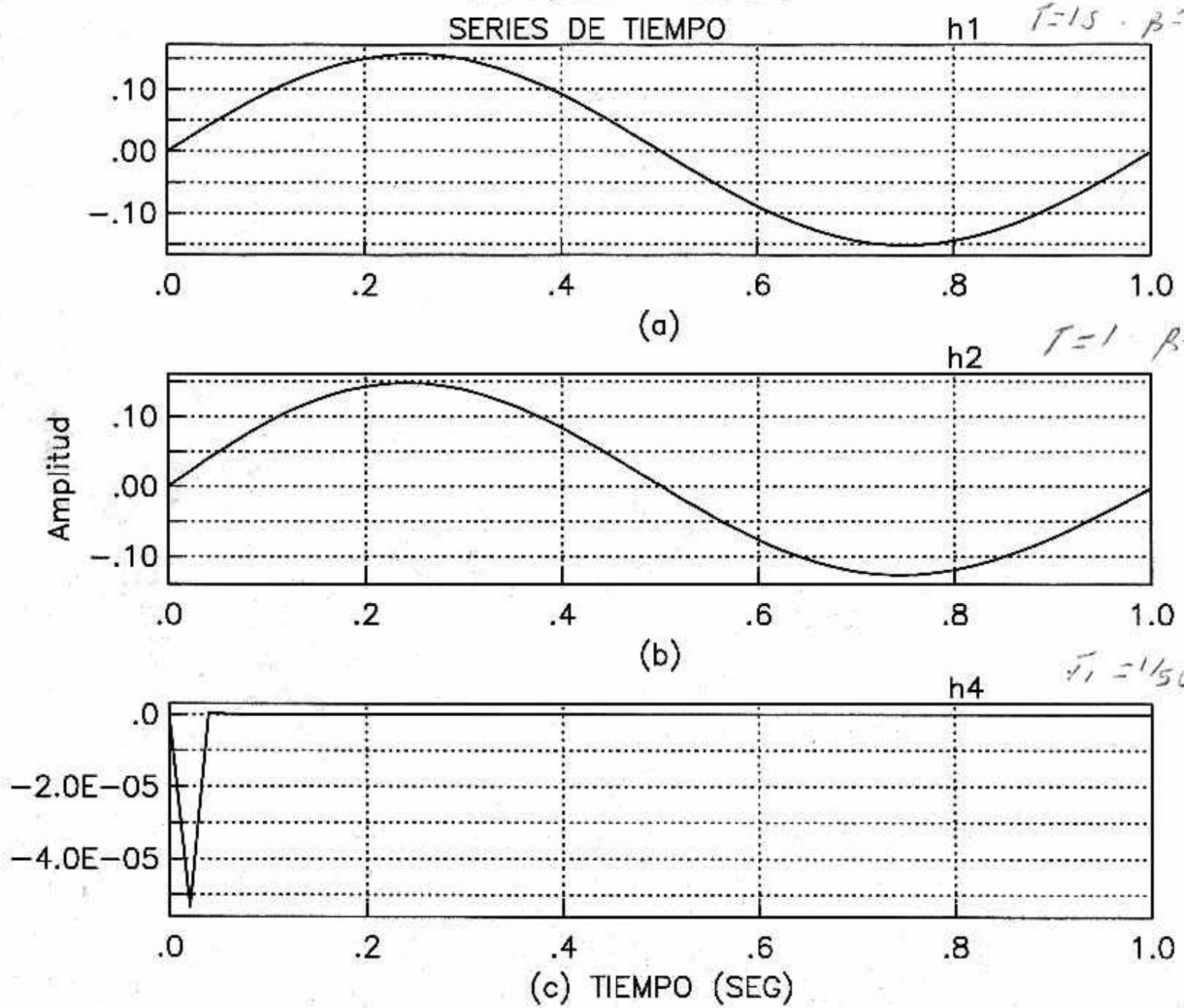

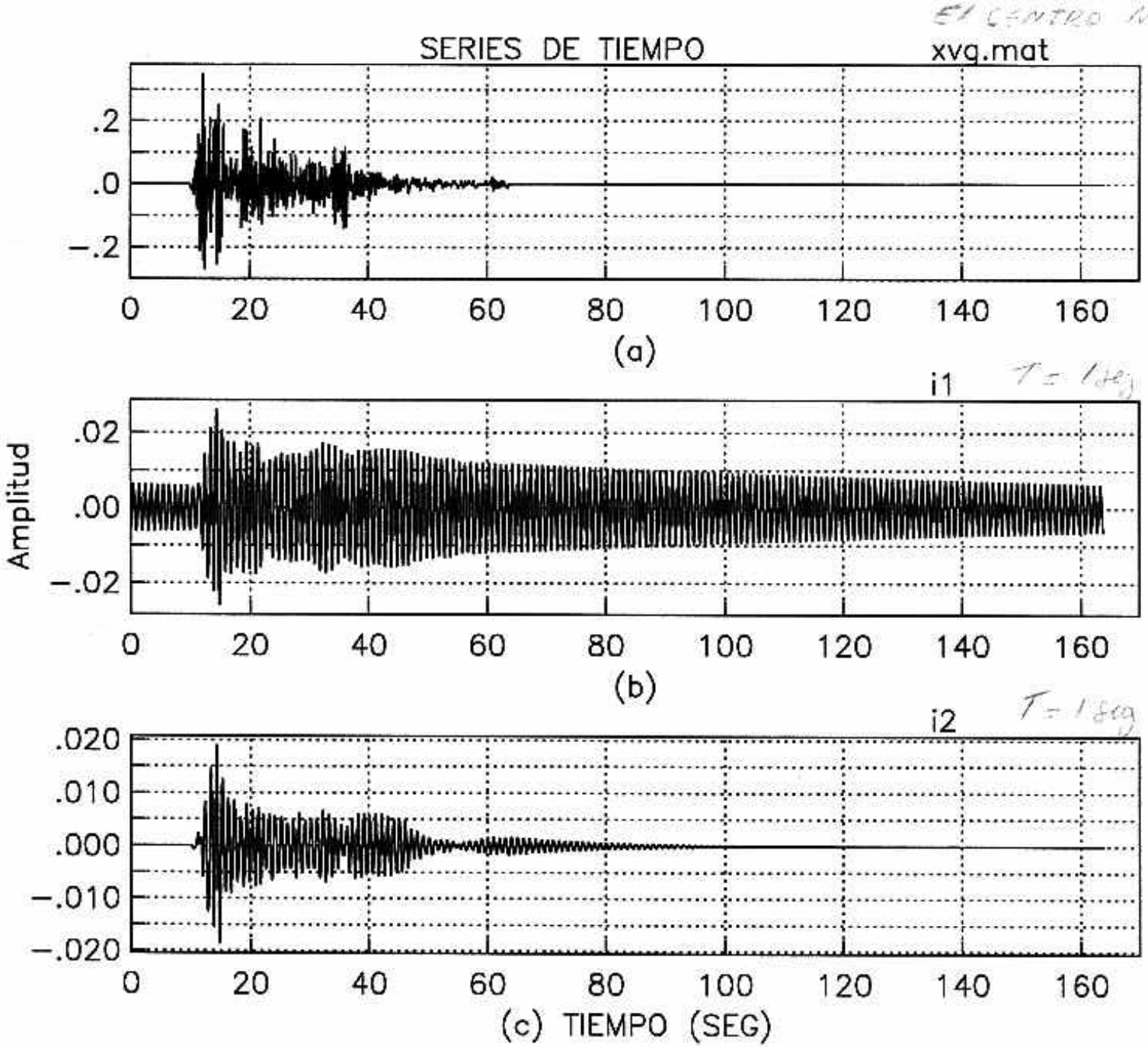
SERIES DE TIEMPO
xvg.mat
.2
.0
−.2
0
20
40
60
80
100
120
140
160
(a)
i1
Amplitud
.02
.00
−.02
0
20
40
60
80
100
120
140
160
(b)
i2
.020
.010
.000
−.010
−.020
0
20
40
60
80
100
120
140
160
(c) TIEMPO (SEG)

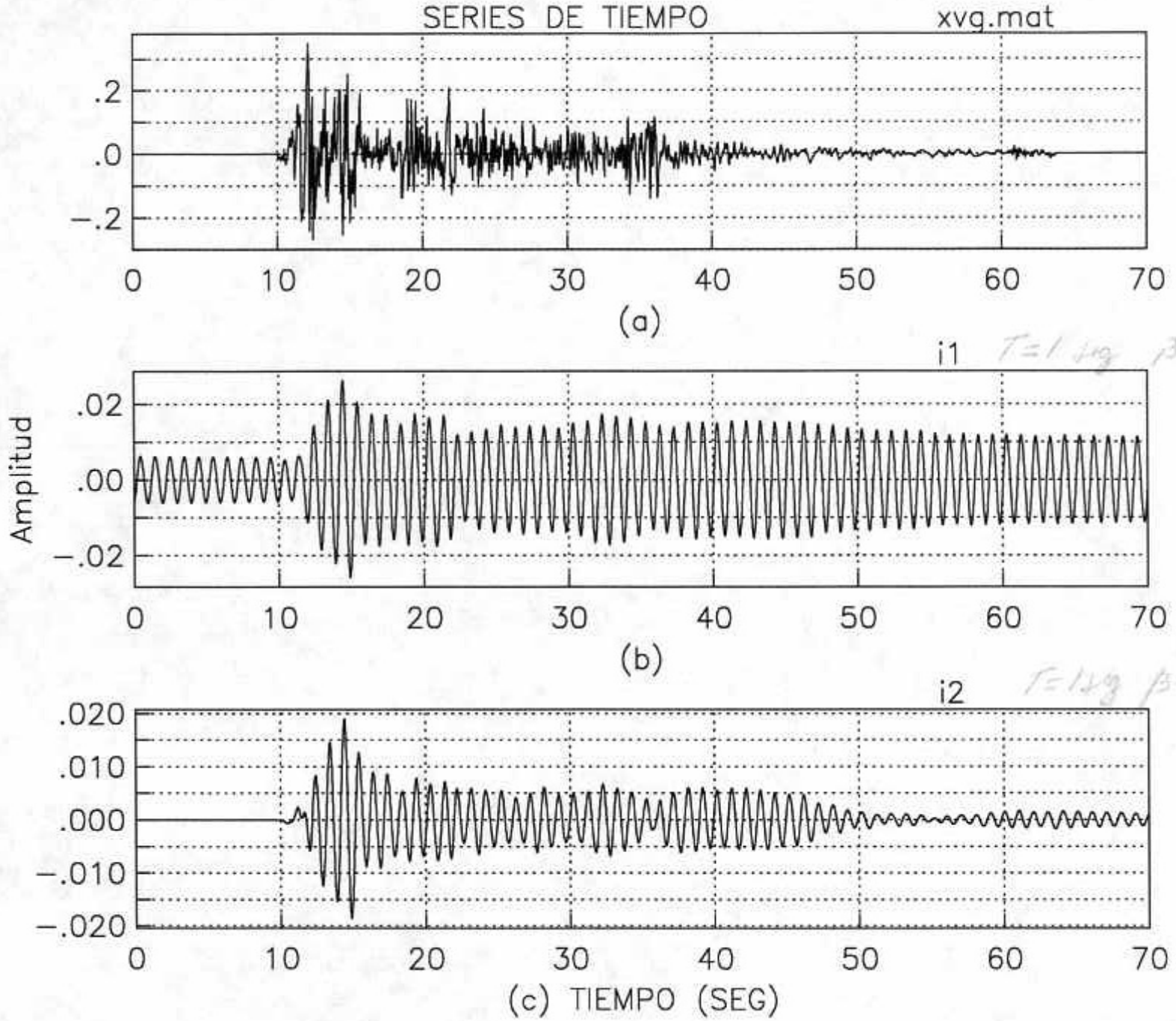
SERIES DE TIEMPO
xvg.mat
.2
.0
−.2
0
10
20
30
40
50
60
70
(a)
i1
Amplitud
.02
.00
−.02
0
10
20
30
40
50
60
70
(b)
i2
.020
.010
.000
−.010
−.020
0
10
20
30
40
50
60
70
(c) TIEMPO (SEG)